

# Separating above canopy CO<sub>2</sub> and O<sub>2</sub> measurements into their atmospheric and biospheric signatures

Kim A. P. Faassen<sup>1</sup>, Jordi Vilà-Guerau de Arellano<sup>1,2</sup>, Raquel González-Armas<sup>1</sup>, Bert G. Heusinkveld<sup>1</sup>, Ivan Mammarella<sup>3</sup>, Wouter Peters<sup>1,4</sup>, and Ingrid T. Lujckx<sup>1</sup>

<sup>1</sup>Meteorology and Air Quality, Wageningen University and Research, Wageningen, the Netherlands

<sup>2</sup>Atmospheric Chemistry Department, Max Planck Institute for Chemistry, 55128 Mainz, Germany

<sup>3</sup>Institute for Atmospheric and Earth System Research (INAR) / Physics, Faculty of Science, University of Helsinki, Helsinki, Finland

<sup>4</sup>University of Groningen, Centre for Isotope Research, Energy and Sustainability Research Institute Groningen, Groningen, the Netherlands

**Correspondence:** Kim Faassen (kim.faassen@wur.nl)

**Abstract.** Atmospheric tracers are often used to interpret the local CO<sub>2</sub> budget, where measurements at a single height are assumed to represent local flux signatures. Alternatively, these signatures can be derived from direct flux measurements or using fluxes derived from measurements at multiple heights. In this study, we contrast interpretation of surface CO<sub>2</sub> exchange from tracer measurements at a single height versus measurements at multiple heights.

5 Specifically, we analyse the ratio between atmospheric O<sub>2</sub> and CO<sub>2</sub> (exchange ratio, ER) above a forest. We consider two alternative approaches: the exchange ratio of the forest (ER<sub>forest</sub>) obtained from the ratio of the surface fluxes of O<sub>2</sub> and CO<sub>2</sub>, derived from measurements at multiple heights, and the exchange ratio of the atmosphere (ER<sub>atmos</sub>) obtained from changes in the O<sub>2</sub> and CO<sub>2</sub> mole fractions over time measured at a single height. We investigate the diurnal cycle of both ER signals, to better understand the biophysical meaning of the ER<sub>atmos</sub> signal. We have combined CO<sub>2</sub> and O<sub>2</sub> measurements from Hyytiälä,  
10 Finland during spring and summer of 2018 and 2019 with a conceptual land-atmosphere model to investigate the behavior of ER<sub>atmos</sub> and ER<sub>forest</sub>. We show that the CO<sub>2</sub> and O<sub>2</sub> signals and their resulting ERs are influenced by climate conditions, such as variations in the soil moisture and temperature, for example during the 2018 heatwave. We furthermore show that the ER<sub>atmos</sub> signal obtained from single height measurements rarely represents the forest exchange directly, mainly because it is influenced by entrainment of air from the free troposphere into the atmospheric boundary layer. The influence of these larger  
15 scale processes can lead to very high ER<sub>atmos</sub> values (even larger than 2), especially in the early morning. These high values do not directly represent carbon cycle processes, but are rather a mixture of different signals.

We conclude that the ER<sub>atmos</sub> signal only provides a weak constraint on local scale surface CO<sub>2</sub> exchange, and that ER<sub>forest</sub> above the canopy should be used instead. Single height measurements always require careful selection of the time of day and should be combined with atmospheric modelling to yield a meaningful representation of forest carbon exchange. More  
20 generally, we recommend always measuring at multiple heights when using multi-tracer measurements to study surface CO<sub>2</sub> exchange.

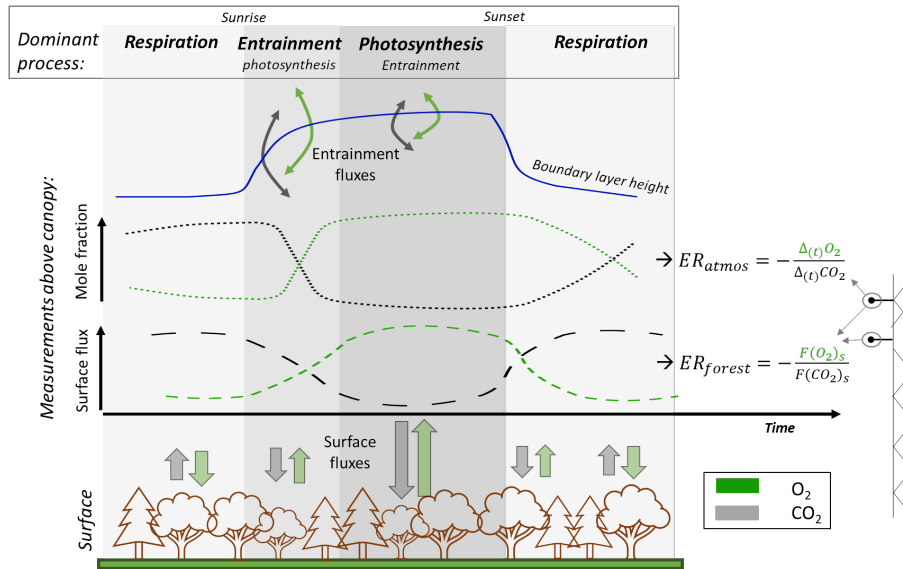


**Figure 1.** Schematic overview of the diurnal cycles of the surface fluxes and mole fractions of atmospheric  $O_2$  and  $CO_2$  above a forest canopy. The figure illustrates the dominant processes throughout the day, with forest exchange dominating the nocturnal and afternoon periods, while early morning signals are primarily influenced by entrainment of air from the residual layer or the free troposphere. The surface fluxes of  $O_2$  and  $CO_2$  result in the Exchange Ratio signal of the forest ( $ER_{forest}$ ), while the changes in the mole fractions of  $O_2$  and  $CO_2$  over time can lead to variations of the Exchange Ratio signal of the atmosphere ( $ER_{atmos}$ ). Note that the term "surface fluxes" refers to the fluxes from the surface layer, which includes the vegetation layer, including the top of the canopy. The surface layer is the lowest 10% of the boundary layer where the surface directly influences the atmospheric boundary layer.

## 1 Introduction

Rising atmospheric carbon dioxide ( $CO_2$ ) levels, resulting from fossil fuel combustion and land use change emissions, moderated by uptake by the terrestrial biosphere and oceans, require a comprehensive assessment of the carbon exchange at local and global scales (Friedlingstein et al., 2022). Atmospheric oxygen ( $O_2$ ) serves as a valuable tracer, enhancing our understanding of carbon exchange due to the close linkage between  $O_2$  and carbon dioxide ( $CO_2$ ) in carbon cycle processes such as fossil fuel combustion, photosynthesis and respiration (Manning and Keeling, 2006; Worrall et al., 2013; Keeling and Manning, 2014; Bloom, 2015; Hilman et al., 2022). The Exchange Ratio ( $ER = -O_2/CO_2$ ), denoted as the number of moles of  $O_2$  exchanged per mole of  $CO_2$ , represents the specific link between  $O_2$  and  $CO_2$  for different processes (Keeling et al., 1998). Long-term  $O_2$  and  $CO_2$  measurements allow us to derive the global ocean carbon sink (Stephens et al., 1998; Rödenbeck et al., 2008; Tohjima et al., 2019) and to estimate changes in fossil fuel emissions (Pickers et al., 2022; Ishidoya et al., 2020; Rödenbeck et al., 2023).

For global applications, a constant ER of 1.1 [ $mol\ mol^{-1}$ ] is assumed for the terrestrial biosphere (Severinghaus, 1995). However, the ER of terrestrial biosphere exchange is not uniform at smaller scales; it varies between ecosystems and over time

35 (Angert et al., 2015; Bloom, 2015; Battle et al., 2019; Hilman et al., 2022). Measuring the ERs of ecosystems and the underlying gross processes facilitates the partitioning of Net Ecosystem Exchange (NEE) into Gross Primary Production (GPP) and Total Ecosystem Respiration (TER) (Ishidoya et al., 2015; Faassen et al., 2023) which is still challenging (Reichstein et al., 2005). The ER for net ecosystem exchange can be determined from the ratio of the net turbulent surface fluxes of  $O_2$  and  $CO_2$  above the canopy, referred to as  $ER_{forest}$  (see Figure 1). The  $O_2$  surface fluxes can be inferred from the vertical gradient: the difference between  $O_2$  mole fraction measurements at multiple heights, together with a turbulent exchange coefficient. Currently, available instruments do not allow Eddy Covariance (EC)  $O_2$  measurements. The  $ER_{forest}$  signal predominantly represents forest exchange occurring in and below the canopy (small scale processes), comprising the individual ERs of TER ( $ER_r$ ) and GPP ( $ER_a$ ) (Ishidoya et al., 2013, 2015; Faassen et al., 2023). Alternatively, net ecosystem ERs have been estimated based on measurements of  $O_2$  and  $CO_2$  mole fractions in the atmosphere at a single height above the canopy. This is referred to as  $ER_{atmos}$  (Figure 1) and is defined as the change in  $O_2$  and  $CO_2$  mole fractions over time (Seibt et al., 2004; Battle et al., 2019; Faassen et al., 2023).

In our recent study (Faassen et al., 2023), we showed a comprehensive comparison of the diurnal behaviour of  $ER_{forest}$  and  $ER_{atmos}$  using measurements collected above a boreal forest in Hyytiälä, Finland. Our analysis revealed that during the afternoon (the photosynthesis dominant period in Figure 1), the  $ER_{atmos}$  signal approaches the  $ER_{forest}$  value, although they did not converge completely. Furthermore, we showed that during the entrainment-dominant period (see Figure 1), the  $ER_{atmos}$  signal strongly exceeded the expected ER value for biosphere exchange, which is typically around 1.1 (Severinghaus, 1995), and even surpassed 2.0. Such high ER values ( $>2.0$ ) cannot be attributed to a single process such as photosynthesis, respiration or fossil fuel combustion, as their ER values are below 2.0. We proposed that the high  $ER_{atmos}$  signal was likely influenced by large scale processes, specifically the entrainment of air from the free troposphere into the boundary layer (Faassen et al., 2023). Also Seibt et al. (2004) and Yan et al. (2023) argue that  $ER_{atmos}$  cannot capture the ER signal of a forest. In contrast, in the studies by Ishidoya et al. (2013, 2015)  $ER_{forest}$  and  $ER_{atmos}$  do result in similar values when small scale processes dominate over large scale processes. In Faassen et al. (2023) we concluded that an atmospheric model was needed to interpret the observed diurnal signals of  $ER_{atmos}$  and  $ER_{forest}$ . The current study delivers this model-based analysis.

60 Until now atmospheric  $O_2$  above forest canopies has primarily been modeled with relatively simple one-box models that use only the surface components, lacking implementation of boundary layer dynamics such as entrainment and boundary layer growth (Seibt et al., 2004; Ishidoya et al., 2013). Understanding how mole fractions, and consequently how  $ER_{atmos}$  evolves throughout the day requires accounting for these critical processes. Yan et al. (2023) recently modelled  $O_2$  and  $CO_2$  within and below a canopy using a multi-layer model and showed that  $ER_{atmos}$  and  $ER_{forest}$  have diurnal and annual patterns. However,  $ER_{atmos}$  was treated as a constant value above the canopy and boundary layer dynamics were not accounted for. To expand on the work by Yan et al. (2023) and gain further insight into the diurnal  $ER_{atmos}$  behaviour above a canopy, in this study we use the mixed layer model Chemistry Land-surface Atmosphere Soil Slab (CLASS) (Vilà-Guerau de Arellano et al., 2015). In short, the model is able to represent the thermodynamics and biophysical processes associated with the diurnal variation

70 in the boundary layer and can provide insights into the processes contributing to  $ER_{atmos}$  formation. Additionally, the model facilitates the analysis of  $ER_{atmos}$  behavior under more extreme conditions such as droughts or heatwaves.

In this study, we aim to enhance our understanding of single height  $O_2$  and  $CO_2$  measurements and the resulting  $ER_{atmos}$  signal, as observed above the canopy, and we propose a new relationship between the  $ER_{atmos}$  and  $ER_{forest}$  signal. We seek  
75 to determine whether single height  $O_2$  and  $CO_2$  measurements can be employed to estimate the ecosystem's ER despite the aforementioned limitations. Additionally, we explore whether the  $ER_{atmos}$  signal constrains boundary layer dynamics, and we identify cases where large scale processes (e.g. entrainment of background air) influence the signal of small scale processes (e.g. NEE) by analyzing different diurnal regimes of  $ER_{forest}$  and  $ER_{atmos}$ . We combine measurements from campaigns in Hyytiälä, Finland during the spring/summer of 2018 and 2019 with an analysis of the mixed layer model CLASS. This combined ap-  
80 proach allows us to address the following research questions: 1) When does  $ER_{atmos}$  represent local forest exchange processes, and become equal to  $ER_{forest}$ ? and 2) What is the underlying physical explanation for the high  $ER_{atmos}$  values observed in the recent study by Faassen et al. (2023)?

In this paper we first derive a theoretical relationship between  $ER_{atmos}$  and  $ER_{forest}$  that can help us to understand which  
85 components influence the diurnal cycle of  $ER_{atmos}$  and when  $ER_{atmos}$  should indicate the same processes as  $ER_{forest}$  (Sect. 2). To evaluate the diurnal cycle of  $ER_{atmos}$  we combine observational data with the CLASS model (Sect. 3). We then show the model evaluation and the  $ER_{atmos}$  and  $ER_{forest}$  model results in Sect. 4.2 and we analyse different cases to explain the diurnal behaviour of  $ER_{atmos}$  during distinct periods of the day and investigate when  $ER_{atmos}$  represents forest exchange (Sect. 4.3). Next, we place our results in perspective and show how  $ER_{atmos}$  should (not) be used (Sect. 5). Finally, we present our  
90 conclusions on the physical explanations for the differences between the diurnal behaviour of both  $ER_{atmos}$  and  $ER_{forest}$ .

## 2 Fundamental concepts

### 2.1 The mixed layer theory

The land-atmosphere model CLASS (Vilà-Guerau de Arellano et al., 2015) is based on the mixed-layer theory which assumes that scalars (such as  $O_2$ ,  $CO_2$ ,  $\theta$ ) are constant with height in the atmospheric boundary layer (Lilly, 1968; Tennekes, 1973).  
95 Figure 2 illustrates these assumptions for potential temperature ( $\theta$ ),  $O_2$  and  $CO_2$ . Within the mixed layer theory, no distinct surface layer exists, and a capping inversion links the mixed layer value (the bulk constant value) with the lapse rate of the free troposphere. This inversion, termed the 'jump' ( $\Delta_{(ft-bl)}$ ), represents the difference of a scalar (e.g. the  $CO_2$  mole fraction) between the atmospheric boundary layer and the free troposphere. The free troposphere is represented by a linear change of the scalar with height (the lapse rate).

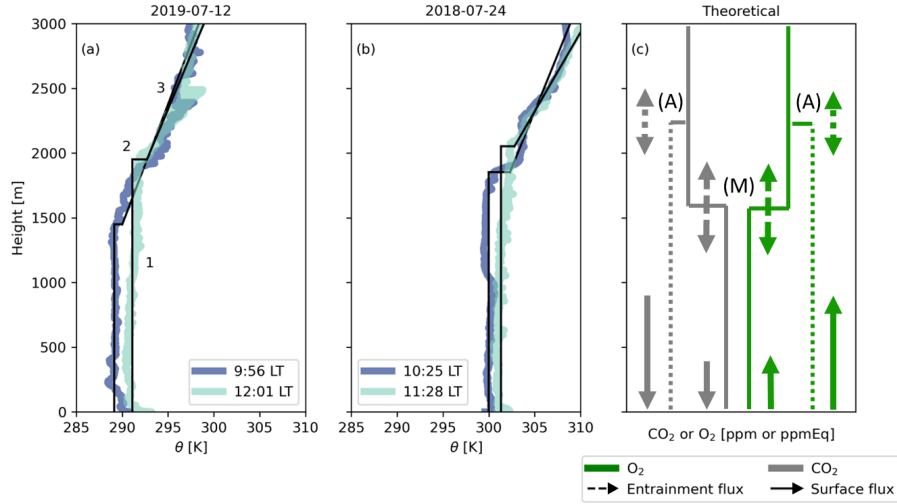


**Figure 2.** Vertical profiles of potential temperature ( $\theta$ ) measured by radiosondes at Hyytiälä on 12 July 2019 (a) and 24 July 2018 (b). The observations are conceptualized (black lines) to show: 1) the well-mixed profiles at different time steps, 2) the jump between the boundary layer and the free troposphere, and 3) the lapse rate in the free troposphere. 1, 2 and 3 are used to initialize the CLASS model. (c) gives the theoretical vertical profiles of  $O_2$  and  $CO_2$  for the early morning (M) and late afternoon (A). The sizes of the arrows indicate the effects of entrainment (dashed lines) and the surface fluxes (solid lines) on the vertical profiles.

CLASS describes the well-mixed layer with a scalar constant in height (Figure 2). This scalar ( $\phi$ ) can then be solved in the mixed-layer with the following equations (Vilà-Guerau de Arellano et al., 2015):

$$\frac{\partial \phi}{\partial t} = \frac{(\overline{w'\phi'})_s - (\overline{w'\phi'})_e}{h} - adv(\phi) \quad (1)$$

where  $\partial \phi / \partial t$  is the tendency (i.e. change over time) of a generic well-mixed scalar,  $w'$  are the deviations of the mean for  $w$  which is the vertical wind speed, and  $\phi'$  are the deviations from the mean for a scalar  $\phi$ . The term  $(\overline{w'\phi'})_s$  is the surface flux of  $\phi$  and represents the small scale processes,  $(\overline{w'\phi'})_e$  is the entrainment flux,  $h$  is the boundary layer height and  $adv(\phi)$  is the horizontal advection of scalar  $\phi$  into the well-mixed layer.  $(\overline{w'\phi'})_e$  and  $adv(\phi)$  represent large scale processes, in contrast to the local surface exchange  $(\overline{w'\phi'})_s$ .

The entrainment flux is dependent on the entrainment velocity and the jump:

$$(\overline{w'\phi'})_e = -w_e \cdot \Delta_{(ft-bl)}\phi = \left( \frac{\partial h}{\partial t} - w_{sub} \right) \cdot \Delta_{(ft-bl)}\phi \quad (2)$$

where  $w_e$  is the entrainment velocity,  $\Delta_{(ft-bl)}\phi$  is the jump between the free troposphere and the atmospheric boundary layer, and  $w_{sub}$  is the mean vertical subsidence velocity associated normally with high pressure systems. We assume  $w_{sub}$  is negligible, because our focus does not lie on the influence of synoptic scale processes.

$\Delta_{(ft-bl)}\phi$  changes over time (see Figure 2) and depends on the surface fluxes and the air that is entrained from the free troposphere (see Equation 1):

$$\frac{\partial\Delta_{(ft-bl)}\phi}{\partial t} = \gamma_\phi \cdot w_e - \frac{\partial\phi}{\partial t} \quad (3)$$

where  $\gamma_\phi$  is the lapse rate of  $\phi$  in the free troposphere, and  $\partial\phi/\partial t$  is the change over time of the well-mixed scalar  $\phi$  (i.e. in the  
120 boundary layer).

Last, the growth of the boundary layer height ( $\frac{\partial h}{\partial t}$ ) effectively determines the entrainment velocity and therefore the entrainment flux of a certain scalar. The growth of the boundary layer is caused by the virtual potential temperature ( $\theta_v$ ), also called buoyancy:

$$125 \quad \frac{\partial h}{\partial t} = -\frac{(\overline{w'\theta'_v})_e}{\Delta_{(ft-bl)}\theta_v} + w_{sub} \quad (4)$$

where  $\theta_v$  is the virtual potential temperature (i.e. potential temperature of dry air) and  $w_{sub}$  is the subsidence velocity. For more details on these equations, see Vilà-Guerau de Arellano et al. (2015) and Sect. 3.2.2 and Sect. A2 for the application of  $O_2$ .

## 2.2 Theoretical relationship between $ER_{atmos}$ and $ER_{forest}$

130 The ER signal of the forest ( $ER_{forest}$ ) is defined as (Faassen et al., 2023):

$$ER_{forest} = -\frac{(F_{O_2})_s}{(F_{CO_2})_s} \approx -\frac{-K_\phi \cdot \Delta_{(z)}O_2/\Delta z}{-K_\phi \cdot \Delta_{(z)}CO_2/\Delta z} \quad (5)$$

where  $(F_{O_2})_s$  and  $(F_{CO_2})_s$  are the mean net turbulent surface fluxes of  $O_2$  and  $CO_2$  respectively over a certain time period above the canopy, and can be derived from the vertical gradient of  $O_2$  ( $\Delta_{(z)}O_2$ ) and  $CO_2$  ( $\Delta_{(z)}CO_2$ ) measurements at two heights together with an exchange coefficient following the K-theory ( $K_\phi$ ) (Faassen et al., 2023). Note that the K-theory does  
135 not apply when one of the measurement levels is inside the canopy. For readability, we write the surface fluxes for both  $O_2$  and  $CO_2$  as  $F_\phi$  instead of  $(\overline{w'\phi'})_s$  that was used above for the general theory.

The ER signal of the atmosphere ( $ER_{atmos}$ ) is defined as (Faassen et al., 2023):

$$ER_{atmos} = -\frac{\partial O_2/\partial t}{\partial CO_2/\partial t} \approx -\frac{\Delta_{(t)}O_2}{\Delta_{(t)}CO_2} \quad (6)$$

140 where  $\Delta_{(t)}O_2$  and  $\Delta_{(t)}CO_2$  are the changes of the  $O_2$  and  $CO_2$  mole fractions over time (tendencies) at a single height. Linear regression between  $O_2$  and  $CO_2$  can be applied and the slope gives the  $ER_{atmos}$  value for a certain event or time period. For this study, a linear regression was applied for the three periods described in Section 4.2.1 for the observations (1 value per 30 minutes) and the CLASS model output (1 value per 10 seconds).

145 According to the mixed-layer theory described above, the tendencies in equation 6 depend on the surface and entrainment fluxes, together with the boundary layer height ( $h$ ) (see Equation 1). Equation 6 can be rewritten by implementing Equation 1:

$$ER_{atmos} = -\frac{((F_{O_2})_s - (F_{O_2})_e)/h}{((F_{CO_2})_s - (F_{CO_2})_e)/h} \quad (7)$$

where  $(F_{O_2})_s$  and  $(F_{CO_2})_s$  are the net surface fluxes of  $O_2$  and  $CO_2$ , and  $(F_{O_2})_e$  and  $(F_{CO_2})_e$  are the entrainment fluxes of  $O_2$  and  $CO_2$  respectively. For simplicity we ignored the advection term in Eq. 1 here, but we will add it later (Eq. 9). As shown  
150 in Eq. 2, the entrainment flux depends on the entrainment velocity ( $w_e$ ) and the jump between the free troposphere and the boundary layer ( $\Delta_{(ft-bl)\phi}$ ). Combining the definition of  $ER_{forest}$  (Eq. 5) with Eq. 2, allows us to rewrite Eq. 7 to:

$$ER_{atmos} = ER_{forest} \cdot \left( \frac{1 + \frac{w_e \cdot \Delta_{(ft-bl)O_2}}{(F_{O_2})_s}}{1 + \frac{w_e \cdot \Delta_{(ft-bl)CO_2}}{(F_{CO_2})_s}} \right) = ER_{forest} \cdot \left( \frac{1 + \beta_{O_2}}{1 + \beta_{CO_2}} \right) \quad (8)$$

where  $\Delta_{(ft-bl)O_2}$  and  $\Delta_{(ft-bl)CO_2}$  are the jumps of  $O_2$  and  $CO_2$  between the free troposphere and the boundary layer, and  $\beta_\phi$  is the ratio between the entrainment flux and the surface flux (Vilà-Guerau de Arellano et al., 2004). Equation 8 shows a  
155 clear relationship between  $ER_{atmos}$  and  $ER_{forest}$  following the mixed-layer theory.

Using the definition of Equation 1, we can extend Equation 8 to include the effect of advection of  $O_2$  ( $adv_{O_2}$ ) and  $CO_2$  ( $adv_{CO_2}$ ), which is next to entrainment, the second important large scale process influencing the  $O_2$  and  $CO_2$  values:

$$ER_{atmos} = ER_{forest} \cdot \left( \frac{1 + \beta_{O_2} + \frac{h}{(F_{O_2})_s} \cdot adv_{O_2}}{1 + \beta_{CO_2} + \frac{h}{(F_{CO_2})_s} \cdot adv_{CO_2}} \right) \quad (9)$$

160 Note that in this paper, we mostly focus on cases without advection. We do include it here for completeness and discuss the influence of advection in Section 5.2.

In Appendix A1 we analyse Equation 8 by determining when  $ER_{atmos}$  would theoretically be close to  $ER_{forest}$  during the day. We show that the  $\beta$  values are of particular importance here: when the  $\beta$ 's of  $O_2$  and  $CO_2$  are equal or very small,  $ER_{atmos}$  gives the same signal as  $ER_{forest}$ . To fully unravel the diurnal variations of  $ER_{atmos}$  under realistic conditions and identify influencing  
165 factors, we need to analyse a real case. Therefore, we study two observed situations by means of the coupled land-atmosphere model, CLASS which we will describe in Sect. 3.2.

### 3 Methods

In this section we describe the measurements that were used in this study, together with the mixed-layer model used to evaluate the  $ER_{atmos}$  and  $ER_{forest}$  signals.

170

#### 3.1 Hyytiälä 2018 and 2019 measurement campaigns

The observational data were obtained from the SMEAR II Forestry Station of the University of Helsinki in Finland, located in Hyytiälä, Finland (61° 51'N, 24° 17'E, +181 MSL) (Hari et al., 2013). The SMEAR II station serves as a measurement

175 site within a boreal forest equipped with a 128 m tower for continuous measurements of atmospheric variables, fluxes and  
greenhouse gas mole fractions. These data are accessible at <https://smear.avaa.csc.fi/>. The tower is situated in a homogeneous  
Scots pine forest, with an average canopy height of 18 m and a podzolic soil. The measurement site is predominantly influ-  
enced by the surrounding forest and has minimal impact from signals of fossil fuel combustion (Faassen et al., 2023). For a  
comprehensive description, see Hari et al. (2013).

180 During the spring/summer of 2018 (03-Jun until 02-Aug) and 2019 (10-Jun until 17-Jul), two measurement campaigns, re-  
ferred to as OXHYYGEN (Oxygen in Hyytiälä), were conducted at Hyytiälä. Continuous measurements of both O<sub>2</sub> and CO<sub>2</sub>  
mole fractions were taken at two heights (125 m and 23 m). O<sub>2</sub> was measured using an Oxzilla II fuel cell analyser, and CO<sub>2</sub>  
was measured with a non-dispersive infrared (NDIR) photometer (URAS26). Further details about these measurements and  
the measurement system are given in Faassen et al. (2023). The measurement precision for O<sub>2</sub> was 19 per meg and for CO<sub>2</sub>, it  
185 was 0.07 ppm. Although the precision for O<sub>2</sub> is relatively poor compared to previous studies, it is still adequate for studying  
the diurnal time scale, as shown in Faassen et al. (2023).

O<sub>2</sub> measurements are typically expressed as  $\delta\text{O}_2/\text{N}_2$  ratios in ‘per meg’ units due to the high abundance of O<sub>2</sub> in the atmo-  
sphere (20.946%), classifying it as a non-trace gas. For direct comparison with CO<sub>2</sub> and implementation into our model, we  
190 convert per meg to ppm equivalents (ppmEq) by multiplying with the standard mole fraction of O<sub>2</sub> in air of 0.20946 (Keeling  
et al., 1998).

During the OXHYYGEN campaigns, radiosondes were launched on multiple days several times per day to quantify the  
impact of boundary-layer dynamics on the O<sub>2</sub> and CO<sub>2</sub> diurnal cycles. The radiosondes (Windsond, model S1H3-R, Sweden)  
195 measured vertical profiles of air pressure, wind speed, wind direction, relative humidity and temperature, with flight heights  
reaching a maximum of 4500 m and rising rate of about 1.7 m s<sup>-1</sup>. The measurements have an accuracy of 1.0 hPa for air pres-  
sure, 5% for wind speed, 0.2 C for temperature and 1.8% for the relative humidity. The temperature and humidity probe has a  
response time of 6 seconds, effectively averaging over about 10 m of altitude. For our analysis, we computed vertical profiles of  
potential temperature ( $\theta$ ) and specific humidity ( $q$ ) based on pressure, temperature and relative humidity measurements. Based  
200 on the vertical profile of vertical temperature, we also determine the boundary layer height with the parcel method (Kaimal and  
Finnigan, 1994). Figure 2 shows examples of vertical profile measurements of  $\theta$  for July 12, 2019, and July 24, 2018.

## 3.2 Modelling setup in CLASS

### 3.2.1 Implementation of CO<sub>2</sub> in CLASS

205 CLASS serves as a fundamental tool that enables further understanding of specific processes within the atmospheric boundary  
layer. Several studies have shown that CLASS is successful in reproducing observational data (Vilà-Guerau de Arellano et al.,



2012, 2019; Schulte et al., 2021). The study of Ouwensloot et al. (2012) specifically showed that CLASS is able to reproduce the boundary dynamics at the Hyytiälä measurement site. Within CLASS, the vegetation is described using a big-leaf model. The surface stomatal conductance that is representative for the canopy is up-scaled from leaf stomatal conductance by integrating over the leaf area index and incorporating soil moisture. The leaf stomatal conductance is calculated with the A-gs model. The A-gs model relates leaf stomatal conductance ( $g_s$ ) to the net leaf  $CO_2$  assimilation ( $A$ ) (Jacobs et al., 1996; Ronda et al., 2001). The model computes the dependence of  $g_s$  and  $A$  with the internal  $CO_2$  mole fraction, the amount of light, the atmospheric temperature, the vapor pressure deficit, and the soil water content at the root zone. Finally, the canopy net  $CO_2$  assimilation is obtained with a function that is inspired by Fick's law of diffusion, based on the difference of the atmospheric  $CO_2$  and the internal  $CO_2$  mole fractions, the aerodynamic resistance and the surface stomatal conductance. The soil respiration is implemented as a function of soil temperature and soil moisture (Vilà-Guerau de Arellano et al., 2012). Combining the net assimilation ( $A_n$ ) of the plants on canopy level and the soil respiration flux results in the net ecosystem exchange (NEE). This means that the model does not produce exactly the GPP and TER fluxes. The differences between  $A_n$  and GPP, and soil respiration and TER are not directly relevant for our study and we therefore refer to GPP and TER in the following Sections, as these terms are more commonly used in the atmospheric  $CO_2$  community. The water cycle is connected to the  $CO_2$  cycle through the surface stomata and the soil moisture inhibition functions for assimilation and respiration.

### 3.2.2 Implementation of $O_2$ in CLASS

To model both  $ER_{forest}$  and  $ER_{atmos}$ , we incorporated the surface flux and the atmospheric mole fraction of  $O_2$  into the CLASS model. We represent the surface flux of  $O_2$  by multiplying the ER of assimilation ( $ER_a$ ) and the ER of respiration ( $ER_r$ ) with the CLASS-calculated  $CO_2$  fluxes at the canopy scale. We used the observationally derived  $ER_a$  and  $ER_r$  values as previously determined in Faassen et al. (2023) for the same site, which were 0.96 and 1.03 respectively. The net surface flux of  $O_2$  was then resolved with the following equation:

$$F(O_2)_s = F_{CO_2(a)} \cdot -ER_a + F_{CO_2(r)} \cdot -ER_r \quad (10)$$

where  $F(O_2)_s$  is the net  $O_2$  surface flux above the canopy,  $F_{CO_2(a)}$  is the net assimilation flux and  $F_{CO_2(r)}$  is the soil respiration flux. The change of atmospheric  $O_2$  over time was resolved with Equation A1 (similar to Equation 1) and the entrainment flux is based on Equation A2 (see also Equation 2). Note that the  $ER_a$  from Faassen et al. (2023) was based on GPP fluxes and this  $ER_a$  is now linked to the net assimilation flux (GPP minus the photo and dark respiration) of the model (Jacobs et al., 1996; Ronda et al., 2001). Seibt et al. (2004) and Ishidoya et al. (2013) showed that  $ER_a$  values based on net assimilation have similar values compared to the 0.96 based on GPP. We therefore expect that this discrepancy will not influence our results.

It is important to note that the resulting  $ER_{forest}$  signal is not the (weighted) average between  $ER_a$  and  $ER_r$ , as was also shown by Faassen et al. (2023). The  $ER_{forest}$  signal results from the TER and GPP fluxes with different sizes and signs, each with their own ER signals ( $ER_r$  and  $ER_a$  respectively). Figure 3 shows that the resulting  $ER_{forest}$  signal does not necessarily

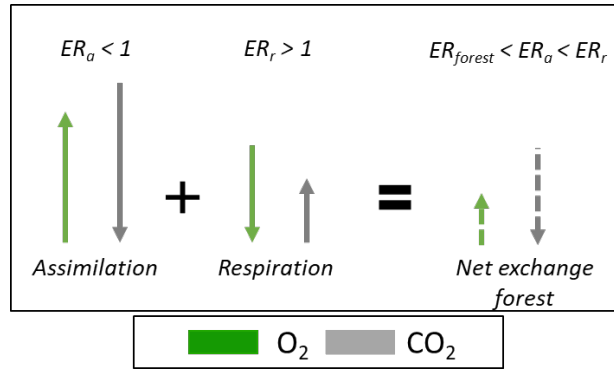


**Figure 3.** Schematic overview of how two processes with different ER signals produce a combined ER signal that is not necessarily the average of the two processes, nor necessarily falls inside the range of the two combined ER signals. This is due to the different signs for the O<sub>2</sub> and CO<sub>2</sub> fluxes. The example is given for combining the ER signal of Assimilation (ER<sub>a</sub>) and Respiration (ER<sub>r</sub>) into ER<sub>forest</sub> and uses values from our study that are by coincidence larger and smaller than 1.

240 fall inside the range of the ER<sub>a</sub> and ER<sub>r</sub> signals because the TER and GPP have opposite signs of the O<sub>2</sub> and CO<sub>2</sub> fluxes. This counter-intuitive situation can also occur for combining signals with different isotopic signatures (Miller and Tans, 2003).

### 3.2.3 Initial conditions

We determined initial and boundary conditions for two cases, to constrain the model to the observations. One case was based on the year 2019 (base case) and the other case was based on the year 2018 (characterized by a warm summer in Finland; Peters et al., 2020; Lindroth et al., 2020). Using the two years to initialize CLASS we were able to better constrain the vegetation's response in the CLASS model under extreme conditions. For each year, we selected one representative day for the initialization and validation of the CLASS model. We used 10-07-2019 for the base case and an aggregate between 28-08-2018 and 29-08-2018 for the warm case. The initial and boundary conditions for the initialisation of the CLASS runs can be found in Tables C2 and C3 in the Appendix. Note that the initial jumps ( $\Delta_{(ft-bl)}$ ) of O<sub>2</sub> and CO<sub>2</sub> are based on the best fit between the model and the observations during the day, as direct observations of the jumps were not available. A detailed discussion can be found in section 5.3.

We deliberately made only minimal adjustments for the initialization of the 2018 case compared to the 2019 base case, to ensure consistency. We assumed that the initial relative humidity remained constant at 80%, regardless of temperature variations, similar to the studies of Vilà-Guerau de Arellano et al. (2012) and van Heerwaarden and Teuling (2014).

We adjusted several parameters of the A-g<sub>s</sub> land surface scheme and the soil respiration to improve the agreement between the surface fluxes of the model and the observations in Hyytiälä for both the base case (2019) and the warmer case (2018) (Table C2). We decreased the mesophyll conductance ( $g_m$ : 2 mm s<sup>-1</sup>) to better match pine forest conditions (Gibelin et al.,

260 2008; ECMWF IV, 2014; Visser et al., 2021). Furthermore, the reference temperature of  $g_m$  ( $T_{2(g_m)}$ : 305 K) was increased to reduce afternoon plant stress and to make the CLASS run more comparable with the observations. Lastly, we adjusted the curvature of the drought response curve ( $c_\beta$ ) from zero to 15% (Combe et al., 2015), given that several studies demonstrate the pine forest in Hyytiälä to be relatively resilient to lower soil moisture values and thus needing a higher ( $c_\beta$ ) value (Gao et al., 2017; Lindroth et al., 2020).

265

### 3.2.4 Sensitivity analyses

We conducted two sensitivity analyses to gain a deeper understanding of the  $ER_{atmos}$  behaviour under varying conditions and to identify factors that lead to a smaller difference between  $ER_{atmos}$  and  $ER_{forest}$ . Specifically, we looked at changes in  $ER_{atmos}$  resulting from changing the different components of Eq. 8. The first sensitivity analysis uses the 2019 base case and investigate  
270 the effect of background air with a different composition by altering the initial jumps of  $O_2$  and  $CO_2$ . By only changing the initial jump and keeping the rest of the 2019 case the same, we simulate situations in which the free troposphere mole fractions of  $O_2$  and  $CO_2$  have changed. In the second sensitivity analysis, we examined the impact of climate conditions by modifying the soil moisture and air temperature, mimicking the conditions observed during the 2018 heatwave. Table C1 presents the variables used for initializing four cases for these two sensitivity studies.

275

## 4 Results

In this results section, we first show our results for the validation of the CLASS model with observations (Section 4.1). Subsequently, we discuss the diurnal variability of both the  $ER_{forest}$  and  $ER_{atmos}$  signals (Section 4.2). We identify three distinct periods throughout the day in which  $ER_{atmos}$  shows large variability (Section 4.2.1). We address the large  $ER_{atmos}$  that we find  
280 in both the observations and the model results (Section 4.2.2). Finally, we perform sensitivity analyses to study the effects of changing large scale conditions, to show that our findings are not only valid for a single day (Section 4.3).

### 4.1 Validation of the $O_2$ and $CO_2$ model results

Overall, the modelled  $O_2$  and  $CO_2$  diurnal cycles match well with the observational data. Figures A3 and A2 in Appendix A3 show that CLASS accurately reproduces the diurnal cycles and captures the  $O_2$  mole fraction changes on a daily time scale for  
285 both 2018 and 2019 (Figure A3b and A3c). The figure shows that the differences between the 2 years are relatively small and indicate that the boundary layer dynamics and the surface fluxes are well represented in CLASS. To accurately replicate the rapid decrease of  $CO_2$  and the sharp increase of  $O_2$  during the rapid growth of the atmospheric boundary layer (between 6:30 and 11:30), we adjusted the jump between the boundary layer and the free troposphere ( $\Delta_{(ft-bl)}$ ) for both  $O_2$  (30 ppmEq) and  $CO_2$  (8 ppm), ensuring that the model aligned with the measurements. Based on values from previous studies, it is realistic  
290 for the  $CO_2$  jump to range between 8 ppm and 40 ppm (Vilà-Guerau de Arellano et al., 2004; Casso-Torralba et al., 2008).

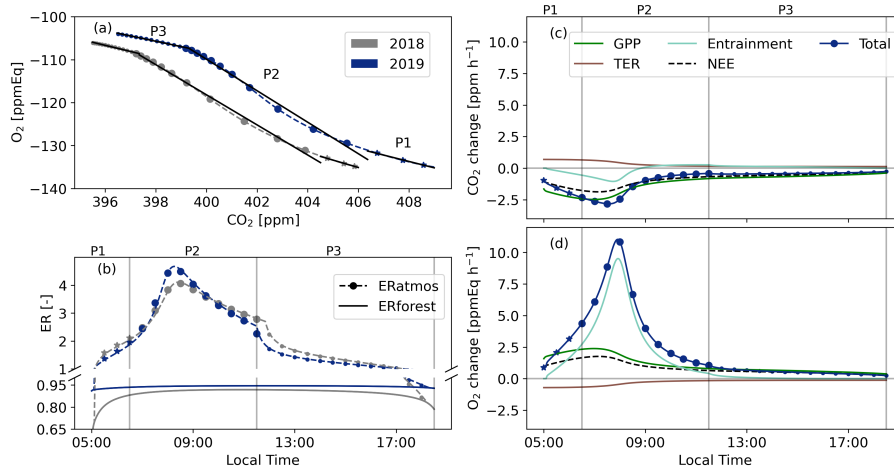


**Figure 4.** Diurnal cycles of  $O_2$  and  $CO_2$  mole fractions (a) and  $ER_{atmos}$  and  $ER_{forest}$  (b) as modelled with CLASS for the selected days in 2018 and 2019. We identify 3 distinct periods; P1 05:00-06:30 LT, P2 06:30-11:30 LT, and P3 11:30-18:30 LT, based on panels c and d, which show the tendencies for the 2019 case (change over time) for  $CO_2$  and  $O_2$  for each process that influences their mole fractions (Equation 1). The symbols represent half hourly averaged values of the CLASS model output.

While there is limited data available to validate the jump of  $O_2$ , based on preliminary results from a campaign in Loobos, the Netherlands, a jump of 30 ppmEq for  $O_2$  seems reasonable. Our chosen combination of  $O_2$  and  $CO_2$  jumps remains an uncertain component in our analysis and will be further discussed in Section 5.3.

## 295 4.2 Diurnal variability of $ER_{atmos}$ and $ER_{forest}$ in 2018 and 2019

In this section, we discuss the diurnal variability of the  $ER_{atmos}$  signal for both the 2018 and 2019 cases. First, we focus on the budget components (GPP, TER and entrainment) that influence the  $O_2$  and  $CO_2$  signals (Section 4.2.1). To complete the analysis, we support the numerical analysis with Equation 8 to gain a more comprehensive understanding of the underlying processes driving the  $ER_{atmos}$  signal for the 2019 case (Section 4.2.2).

### 300 4.2.1 The three distinct periods of the $ER_{atmos}$ signal during daytime

The  $ER_{atmos}$  signals obtained for the 2018 and 2019 experiments display large variability throughout the daytime (panels a and b in Figure 4). We identify three distinct periods during the day based on the processes shown in Figure 4c and 4d: 1) the early morning regime (P1, 5:00-6:30 LT), characterised by an increasing net  $CO_2$  flux into of the forest but a non-growing boundary layer (Figure A3a), during which the  $ER_{atmos}$  signal during P1 is still relatively close to  $ER_{forest}$ ; 2) the entrainment  
 305 dominant period (P2, 6:30-11:30 LT), where air from a residual layer or air masses from the free troposphere are entrained into the boundary layer and significantly influence the signals, leading to large  $ER_{atmos}$  values, with an average greater than

**Table 1.**  $ER_{\text{atmos}}$  values (calculated as the slope of the  $O_2$  and  $CO_2$  mole fractions) and  $ER_{\text{forest}}$  for the selected days in 2018 and 2019 for both observations (Obs) and the CLASS model for the three selected periods (P1: 5:00-06:30 LT, P2: 06:30-11:30 LT and P3: 11:30-19:30 LT). The uncertainties of the observed  $ER_{\text{atmos}}$  and  $ER_{\text{forest}}$  signals are determined following Faassen et al. (2023). Note that due to limited observational data we were unable to derive  $ER_{\text{atmos}}$  values for P1 and P2 in 2018 and for P1 in 2019.

Year	$ER_{\text{atmos}}$ (P1)		$ER_{\text{atmos}}$ (P2)		$ER_{\text{atmos}}$ (P3)		$ER_{\text{forest}}$ (P1-P3)	
	Obs	Model	Obs	Model	Obs	Model	Obs	Model
2018	n.a.	1.72	n.a.	3.50	$1.67 \pm 0.51$	1.43	$0.87 \pm 0.07$	0.90
2019	n.a.	1.48	$3.33 \pm 0.31$	3.66	$1.23 \pm 0.10$	1.24	$0.86 \pm 0.06$	0.94

3 and extreme values reaching close to 5; 3) the afternoon period (P3, 11:30-18:30 LT), where surface processes dominate the observed signals and  $ER_{\text{atmos}}$  moves slowly again towards  $ER_{\text{forest}}$  and become more consistent with values expected for surface processes. The  $ER_{\text{atmos}}$  values during the three identified periods show a good agreement between the observations and  
310 the model results (Table 1). This analysis confirms from a model perspective that values above 2 for  $ER_{\text{atmos}}$ , as we reported in Faassen et al. (2023), are indeed possible. Figures 4c and 4d give first indications on what could cause these high values for  $ER_{\text{atmos}}$ : high influence of entrainment and a different behaviour of the tendencies that influence  $O_2$  compared to  $CO_2$ . In the next Section we discuss the diurnal behaviour of  $ER_{\text{atmos}}$  in more detail by using Equation 8.

315 We find that  $ER_{\text{forest}}$  is much less variable throughout the day than  $ER_{\text{atmos}}$  (Figure 4b). In the early morning and later afternoon the  $ER_{\text{forest}}$  value is lower than the mid-day period. This is caused by an almost equal TER flux (with a higher ER signal) to the GPP flux (with a lower ER signal) caused by low sun light (Figure 3). During mid-day the assimilation of  $CO_2$  by the canopy, with a lower ER signal, becomes increasingly dominant causing the  $ER_{\text{forest}}$  signal to move closer to the  $ER_a$  value.

#### 320 4.2.2 Explanation of the large $ER_{\text{atmos}}$ values

Analysing the diurnal cycle of the different components of Equation 8 for the 2019 case reveals that the peak value of  $ER_{\text{atmos}}$  during P2 is caused by the higher  $\beta$  values (the entrainment flux divided by the surface flux) for  $O_2$  compared to  $CO_2$  (Figure 5). The difference between  $\beta_{O_2}$  and  $\beta_{CO_2}$  is a result of a high  $\Delta_{(ft-bl)}O_2/\Delta_{(ft-bl)}CO_2$  ratio (higher than 3). The terms  $\Delta_{(ft-bl)}O_2$  and  $\Delta_{(ft-bl)}CO_2$  represent the jump across the boundary layer top, and each has a different diurnal cycle caused by a different  
325 surface flux (Figure 5c and 5g). The different diurnal cycles for the jumps lead to an increase in the  $\Delta_{(ft-bl)}O_2/\Delta_{(ft-bl)}CO_2$  ratio, consequently raising the ratio between the  $\beta$  values. This effect is further amplified by a higher surface flux of  $CO_2$  compared to  $O_2$ , caused by an  $ER_{\text{forest}}$  value that is slightly lower than 1. The peak value of  $ER_{\text{atmos}}$  during P2 occurs when both  $w_e$  and the  $\Delta_{(ft-bl)}O_2/\Delta_{(ft-bl)}CO_2$  ratio are high and the surface fluxes are still relatively low. This combination contributes to the distinctive peak in  $ER_{\text{atmos}}$  observed during P2.

330

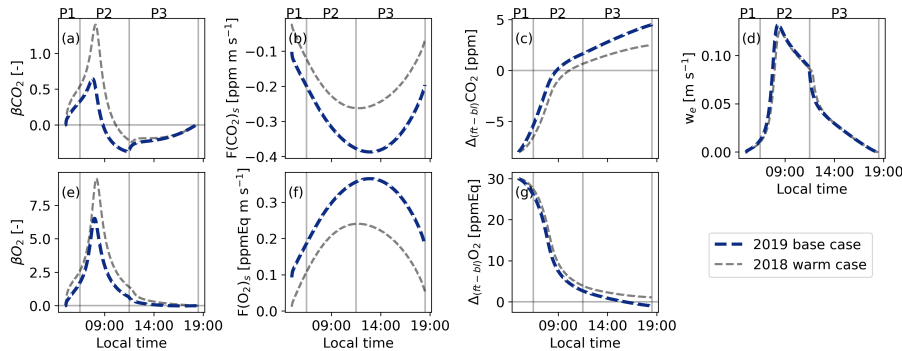


**Figure 5.** The diurnal variability of the different components of Equation 8 for the base case (2019) and the warm case (2018) derived with the CLASS model. (a) and (e) show the  $\beta$  values for  $CO_2$  and  $O_2$ , where  $\beta$  is the entrainment flux divided by the surface flux (Equation 8), (b) and (f) show the net surface flux, (c) and (g) show the jumps between the free troposphere and the boundary layer ( $\Delta_{(ft-bl)}$ ), (d) shows the entrainment velocity ( $w_e$ ). The vertical lines represent three distinct periods: 05:00-06:30 LT (P1), 06:30-11:30 LT (P2), 11:30-18:30 LT (P3).

Later in the afternoon (P3), both  $\beta$  values gradually decrease and become similar, resulting in an  $ER_{atmos}$  signal that becomes closer to  $ER_{forest}$ . This indicates that  $ER_{atmos}$  becomes more representative for surface processes (see also Sect. A1). This decrease in P3 is primarily caused by a reduction in the entrainment velocity ( $w_e$ ) (Figure 5d), indicating a slow growth of the atmospheric boundary layer at end of the day (Figure A3). Additionally, the  $\beta$  values become more similar because  $\Delta_{(ft-bl)O_2}$  moves closer to  $\Delta_{(ft-bl)CO_2}$  during this period (Figure 5c and 5g), caused by the mixing of air with the surface.

The  $ER_{atmos}$  signals exhibit higher values than the theoretical analysis of Sect. A1, because the diurnal cycles of the components of Equation 8 are taken into account (Figure A1 vs Figure 5). Each component of Equation 8 follows its individual diurnal cycle, leading to higher  $ER_{atmos}$  values. Consequently,  $ER_{atmos}$  is integrating individual contributions of several processes, particularly during P2, since it is dominated by the influence of mixing with large scale processes. Careful consideration is needed when interpreting the  $ER_{atmos}$  signal during this period. During P3, the  $ER_{atmos}$  signal appears to align with  $ER_{forest}$  at the end of the day. However, in the 2019 case, this alignment was only observed for a very short period.

We find only small differences for the diurnal behaviour of the  $ER_{forest}$  and  $ER_{atmos}$  signal between the 2018 and 2019 case (Figure 4 and Figure 5). The  $ER_{forest}$  value is lower in 2018 compared to 2019, specifically in the early morning and at the end of the day. This can be attributed to a higher respiration flux caused by the elevated air and soil temperatures during that day in 2018 (Figure A3e). A higher TER flux compared to the GPP flux will decrease the  $ER_{forest}$  value (Figure 3). While we do not have direct measurements of  $ER_r$  and  $ER_a$  for both 2018 and 2019, it is likely that the overall diurnal cycle pattern of  $ER_{forest}$  in Figure 4b (low  $ER_{forest}$  values in the morning and afternoon, higher  $ER_{forest}$  values during mid-day) for both years would have remained consistent. Previous studies suggest that  $ER_r$  is generally higher than  $ER_a$ , even under different atmospheric

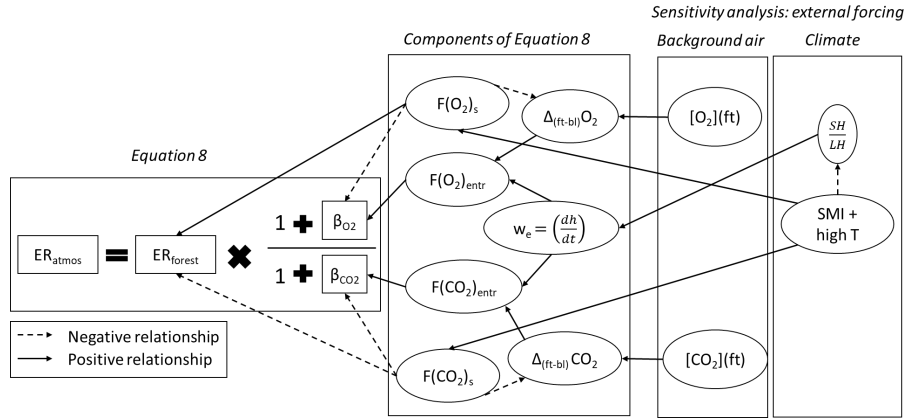


**Figure 6.** The components of Equation 8 and how these influence the  $ER_{atmos}$  signal, including: the exchange ratio of the forest ( $ER_{forest}$ ), the ratio between the net surface flux ( $F_s$ ) and the entrainment flux ( $F_{entr}$ ) which result in the  $\beta$ , the jump between the free troposphere and the boundary layer ( $\Delta_{(ft-bl)}$ ) and the entrainment velocity ( $w_e$ ). The right part of the Figure shows the variables that are changed in the two sensitivity analyses: the background air in the free troposphere ( $[O_2](ft)$  and  $[CO_2](ft)$ ) and the initial Soil Moisture Index (SMI) in combination with a high initial potential temperature ( $\theta_0$ ) that will influence the ratio between the sensible heat flux (SH) and the latent heat flux (LH) at the surface. The dotted arrows indicate a negative influence and the solid arrows indicate a positive influence.

conditions (Angert et al., 2015; Fischer et al., 2015; Hilman et al., 2022). The effect of a warmer and dryer environment on the  $ER_{atmos}$  signal will be further quantified in Sect. 4.3.2 with a more extreme case.

### 4.3 Sensitivity analyses: effects of changing large scale conditions

355 With the next two sensitivity analyses we evaluate whether our findings for the 2019 case are exceptional, or whether they can also occur under different (large scale) conditions. We therefore analyse days with different initial conditions compared to our 2019 and 2018 cases. We focus on the effect of changes in the background air (Sect. 4.3.1) and the effect of changes in the climate conditions (soil moisture and air temperature, Sect. 4.3.2). With these sensitivity analyses we show the complexity of the  $ER_{atmos}$  signal and all the processes that can influence it. Figure 6 is used to illustrate how  $ER_{atmos}$  is formed by the different components of Eq. 8.

360

#### 4.3.1 Effects of changing background air on $ER_{atmos}$

Changing the background air in the free troposphere by decreasing the initial jump ratio or the jump sizes of  $O_2$  and  $CO_2$  compared to the 2019 case, moves the  $ER_{atmos}$  signal closer to  $ER_{forest}$  during P2 and P3 (Figure B1). A lower jump ratio than the 2019 case, but still relatively high jump values ( $\Delta_{(ft-bl)}O_2 = 30$  ppmEq and  $\Delta_{(ft-bl)}CO_2 = -20$  ppm) lead to a decrease in the peak of  $ER_{atmos}$  during P2 and bring  $ER_{atmos}$  closer to  $ER_{forest}$  during P3 (yellow line in Figure B1). As the jump ratio decreases, the  $\beta_{O_2}$  becomes less dominant and closer to  $\beta_{CO_2}$ . When the  $O_2$  and  $CO_2$   $\beta$  values become closer, the  $ER_{atmos}$  value

also moves closer to  $ER_{\text{forest}}$  (Figure 6). However, this does not necessarily mean that the surface has become more dominant since the  $\Delta_{(ft-bl)}$  values are still relatively high.

370 Reducing the jump sizes of both  $O_2$  and  $CO_2$  ( $\Delta_{(ft-bl)}O_2 = 10$  and  $\Delta_{(ft-bl)}CO_2 = -8$ ) still results in a relatively high peak for  $ER_{\text{atmos}}$  during P2 and bring  $ER_{\text{atmos}}$  closer to  $ER_{\text{forest}}$  during P3 (purple line in Figure B1). Including the diurnal cycle of the jumps accounts for the effect that the  $CO_2$  jump changes from a negative to a positive value during the day. When the initial  $CO_2$  jump is lower, the sign change occurs earlier in the day and leads to a more negative  $\beta_{CO_2}$  value. This leads to higher  $ER_{\text{atmos}}$  values during P2 (Figure 6). In contrast, a lower jump size would cause the  $ER_{\text{atmos}}$  signal to move more quickly  
375 towards  $ER_{\text{forest}}$  during P3 because the surface fluxes dominate over the lowered entrainment flux.

Guided by our theoretical and numerical results and constrained by observations, a high  $ER_{\text{atmos}}$  signal during the entrainment dominant period (P2) can therefore be a result of two cases:

1. The  $\Delta_{(ft-bl)}O_2$  is substantially larger compared to  $\Delta_{(ft-bl)}CO_2$  and therefore  $\beta_{O_2}$  dominates over  $\beta_{CO_2}$ .
- 380 2.  $\Delta_{(ft-bl)}CO_2$  changes sign from negative to positive and as a result  $\beta_{CO_2}$  becomes negative resulting in a denominator closer to zero.

Changes in the background air result in a distinct change in the diurnal pattern of  $ER_{\text{atmos}}$ . The difference between the  $ER_{\text{atmos}}$  and  $ER_{\text{forest}}$  signal could therefore provide extra information on the changes of large scale processes. This is further discussed in Sect. 5.2.

385

#### 4.3.2 Effect of climate conditions on $ER_{\text{atmos}}$ and $ER_{\text{forest}}$

By studying the influence of changes in air temperature and soil moisture index (SMI:  $[\text{soil moisture} - w_{\text{wilt}}]/[w_{\text{fc}} - w_{\text{wilt}}]$ ) on the  $ER_{\text{atmos}}$  signal (see Figure 7), we gain insights into how climate conditions can effect  $ER_{\text{atmos}}$  compared to  $ER_{\text{forest}}$ . This allows us to study the effects of seasonality or future climate with dryer and warmer conditions. The 2018 case already showed  
390 how the  $ER_{\text{atmos}}$  signal could change with a decreasing SMI and increasing temperature compared to a more normal year in 2019 (Figure 4 and 5). As a next step, we evaluate the full range of how  $ER_{\text{atmos}}$  could change and how  $ER_{\text{atmos}}$  compares to  $ER_{\text{forest}}$ . Given the same net radiation, a higher SMI enhances soil respiration, photosynthesis and latent heat fluxes, and thus decreases the sensible heat flux because of the energy balance closure, this therefore leads to a smaller boundary layer growth and as a result, decrease the entrainment velocity (see Figure 6). In addition, higher air temperatures accelerate both the photo-  
395 synthesis and the respiration, up to a threshold (Jacobs et al., 1996), resulting in increased GPP and TER fluxes. A lower SMI in combination with higher temperatures can stress plants, leading to decreased  $O_2$  and  $CO_2$  surface fluxes and an enhanced sensible heat flux. This will increase the boundary layer growth and the entrainment velocity (Equation 2 and 4). Note that there are also minor changes for  $ER_{\text{forest}}$  when the SMI and air temperature change as a result of GPP and TER changes.



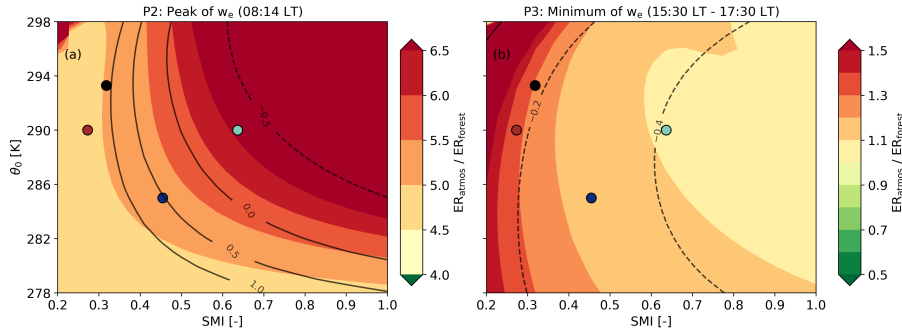


**Figure 7.** Evaluation of the ratio between  $ER_{\text{atmos}}$  and  $ER_{\text{forest}}$  as a function of two key variables that show the effect of a drier and warmer climate: the Soil Moisture Index (SMI) and the initial potential temperature ( $\theta_0$ ). Two moments in the day are analysed, (a) during the maximum value of  $w_e$  at 08:14 LT (P2) and (b) at the end of the day between 15:30 - 17:30 LT when the  $w_e$  is minimal (P3). The grey lines in (a) indicate  $\beta_{\text{CO}_2}$  values, which is the ratio between the entrainment and the surface flux. The grey lines in (b) indicate net  $\text{CO}_2$  surface flux values in  $\text{ppm m s}^{-1}$ . The coloured symbol (brown and light blue) indicate the example cases that are also shown in Figure B2 and the black dot is the 2018 case and the dark blue dot the 2019 case.

400 Increasing or decreasing the SMI in combination with changes in air temperature makes the diurnal variability of  $ER_{\text{atmos}}$  more complex because all the components of Equation 8 are now affected (Figure 6 and Figure 7). We focus on two particular locations in the parameter space shown in Figure 7: a low soil moisture (red symbol) and a high soil moisture case (green symbol), both with higher temperatures compared to the 2019 case (Figure B2).

405 A lower soil moisture of  $0.14 \text{ m}^3 \text{ m}^{-3}$  (SMI = 0.27) with an air temperature of 290 K decreases  $ER_{\text{atmos}}$  during P2 and increases  $ER_{\text{atmos}}$  during P3 compared to the 2019 base case (the red lines in Figure B2 and red symbol in Figure 7). The lower  $ER_{\text{atmos}}$  values during P2 are primarily a consequence of a more dominant entrainment flux. Due to a decrease in the  $\text{O}_2$  and  $\text{CO}_2$  surface fluxes because of stressed plants, both the  $\Delta_{(ft-bl)}$  values for  $\text{O}_2$  and  $\text{CO}_2$  change more slowly and remain high. Higher  $\Delta_{(ft-bl)}$  values, along with a higher entrainment velocity caused by a higher sensible heat flux, lead to elevated entrainment fluxes. By increasing both the  $\text{O}_2$  and  $\text{CO}_2$  entrainment fluxes and decreasing the  $\text{O}_2$  and  $\text{CO}_2$  net surface fluxes, the  $\beta$  values increase and the ratios of the  $\beta$  values move towards the  $\Delta_{(ft-bl)}$  ratios. As a result, the  $ER_{\text{atmos}}$  also moves towards the  $\Delta_{(ft-bl)}$  ratios multiplied with the  $ER_{\text{forest}}$  signal (Figure 6). This is similar to the effect observed when increasing both the initial jumps of  $\text{O}_2$  and  $\text{CO}_2$  (Sect. 4.3.1). The  $\beta$  values stay high during P3 because of the low net  $\text{O}_2$  and  $\text{CO}_2$  surface fluxes. Therefore, the  $ER_{\text{atmos}}$  signal also remains close to the ratio of the  $\Delta_{(ft-bl)}$  values during P3 and the  $ER_{\text{atmos}}$  signal does not  
 415 approach  $ER_{\text{forest}}$  (Figure 6).

In contrast, a higher soil moisture of  $0.22 \text{ m}^3 \text{ m}^{-3}$  (SMI = 0.64) with an air temperature of 290 K increases the  $ER_{\text{atmos}}$  signal during P2 and decreases the  $ER_{\text{atmos}}$  signal during P3 compared to the 2019 base case (the green lines in Figure B2 and

green symbol in Figure 7). This is consistent with the effect observed when lowering the initial  $\Delta_{(ft-bl)}$  value (Sect. 4.3.1).

420

In addition to the conclusions in Sect. 4.3.1 on the causes of the high  $ER_{atmos}$  signals during P2, the sensitivity analyses for changing climate conditions showed that the large differences between  $ER_{atmos}$  and  $ER_{forest}$  at the end of the day (P3) can be caused by:

425

1. A substantially larger  $\Delta_{(ft-bl)}O_2$  compared to  $\Delta_{(ft-bl)}CO_2$  causing  $\beta_{O_2}$  to dominate over  $\beta_{CO_2}$ .
2. High  $\beta_{O_2}$  and  $\beta_{CO_2}$  values because of high  $O_2$  and  $CO_2$  entrainment fluxes and/or low net  $O_2$  and  $CO_2$  surface fluxes.

Our two sensitivity analyses show that several factors, including the entrainment velocity, the  $\Delta_{(ft-bl)}$  values and their ratio and the net surface flux of  $CO_2$  can significantly influence the diurnal behaviour of  $ER_{atmos}$ . When using  $ER_{atmos}$  as an indication of  $ER_{forest}$ , these four factors should be carefully considered. This is crucial to correctly interpret  $ER_{atmos}$  values and to understand the underlying processes that influence the carbon exchange above a forest canopy.

430

## 5 Discussion

In this discussion section, we first address the evaluation of the CLASS model (Section 5.1). Secondly, we elaborate on the issues we found with  $ER_{atmos}$ , and how this value should (and should not) be used (Section 5.2). Thirdly, we discuss the importance of the differences between the free troposphere and boundary layer values for  $O_2$  and  $CO_2$  (Section 5.3). Finally, we put our work in perspective by comparing it to other studies using atmospheric  $O_2$  (Section 5.4) and to studies on other carbon cycle tracers (Section 5.5).

435

### 5.1 Evaluation of the CLASS model

Our implementation of  $O_2$  in the CLASS model could be improved in future studies. Similar to the approach used by Yan et al. (2023), both the  $ER_r$  and  $ER_a$  signals were kept constant and did not account for potential variations under different climate conditions. To advance our understanding of the ER signals over forest canopies, it is crucial to incorporate ER signals that can respond to varying soil and atmospheric conditions. For instance, the  $ER_r$  of the soil respiration depends on air temperature and soil moisture (Hilman et al., 2022; Angert et al., 2015), while the  $ER_a$  is primarily influenced by light on leaf level, and nitrogen availability in the soil (Bloom, 2015; Fischer et al., 2015). Additionally, in our current implementation, we did not include the ER for stem respiration ( $ER_{stem}$ ) (Hilman and Angert, 2016) due to the absence of stem respiration in the CLASS model.

445

While we utilized CLASS in this study as a proof of concept to demonstrate how  $ER_{atmos}$  can change during the day, employing a more elaborate model could allow for more detailed exploration of these  $ER_{atmos}$  dynamics and the contributions of various processes. Models with more vertical levels could simulate vertical gradients and analyze differences in the  $ER_{atmos}$

450 signal at various heights, similar to the approach in Yan et al. (2023). Implementing more vertical levels gives the opportunity to determine the dominance of large scale processes over small scale surface processes at different measurement heights. By incorporating a canopy into the model, the surface resistance could be accounted for, enhancing the accuracy of the modeled surface fluxes. Furthermore, exploring larger temporal and spatial scales could yield valuable insights in the variability of  $ER_{\text{forest}}$  over time and space, in contrast to our CLASS model that is only valid during the day when the SH flux is larger than  
455 zero. Increasing the temporal scale gives the opportunity to improve estimates of  $ER_{\text{forest}}$ . This also has the potential to improve estimates of the global biospheric ER, currently taken to be 1.1 (Severinghaus, 1995).

## 5.2 How $ER_{\text{atmos}}$ should be used

Single height  $O_2$  and  $CO_2$  measurements and their  $ER_{\text{atmos}}$  signal should be analysed very carefully when using it as an indi-  
460 cator for surface exchange. During the complete diurnal cycle,  $ER_{\text{forest}}$  should be utilized as the primary indicator of the ER signals from the surface, while  $ER_{\text{atmos}}$  should not be used for this purpose. In situations where only one height measurement is available, and therefore only  $ER_{\text{atmos}}$  can be obtained, a first estimate of  $ER_{\text{forest}}$  could be made using  $ER_{\text{atmos}}$ . The  $ER_{\text{atmos}}$  signal at the end of the day should then be used to avoid the large influence of entrainment earlier in the day. However, any analysis or discussion based on this estimation should include a comprehensive examination of how entrainment might have  
465 influenced the  $ER_{\text{atmos}}$  signal. This also applies for less representative or non-typical days where the mixed layer theory may be difficult to apply. An example of such case is given by Casso-Torralba et al. (2008), where it is shown that entrainment is still important on a non-typical day, when polluted air is influencing the diurnal  $CO_2$  measurements.

Several studies have showed that  $ER_{\text{atmos}}$  can also serve as an indicator of potential advection from carbon source/sink re-  
470 gions (Ishidoya et al., 2020, 2022a). However, caution should be exercised when directly inferring the specific source based solely on the  $ER_{\text{atmos}}$  value. Equation 9 shows that mixing advected air with the air above a forest will result in an  $ER_{\text{atmos}}$  signal that cannot be directly linked to the source of the advected air. This is because mixing two ER signals with opposite fluxes does not result in a weighted average (Figure 3). Advection of a source with the a known ER signal but with different magnitudes can therefore give different  $ER_{\text{atmos}}$  values. A solution could be to include other tracers in the analysis such as  $NO_x$   
475 or CO (Liu et al., 2023a).

When two or more measurement heights of  $O_2$  and  $CO_2$  are available, and therefore  $ER_{\text{forest}}$  can be derived,  $ER_{\text{atmos}}$  of a single height could be used to provide extra information on large scale processes by analysing the difference between  $ER_{\text{atmos}}$  and the  $ER_{\text{forest}}$  signal. During the day,  $ER_{\text{atmos}}$  provides insights into larger scale processes, while  $ER_{\text{forest}}$  reflects local or  
480 small-scale processes. Therefore, any discrepancy between  $ER_{\text{atmos}}$  and  $ER_{\text{forest}}$  indicates a significant influence of large scale processes. Nonetheless, the exact difference between  $ER_{\text{atmos}}$  from  $ER_{\text{forest}}$  should not be used as an indication of the strength of the influence of large processes. To get more detail on how the large scale processes change between days, the diurnal cycle of  $ER_{\text{atmos}}$  has to be compared during the entrainment dominant period (P2) and the surface dominant periods (P3). During P2,

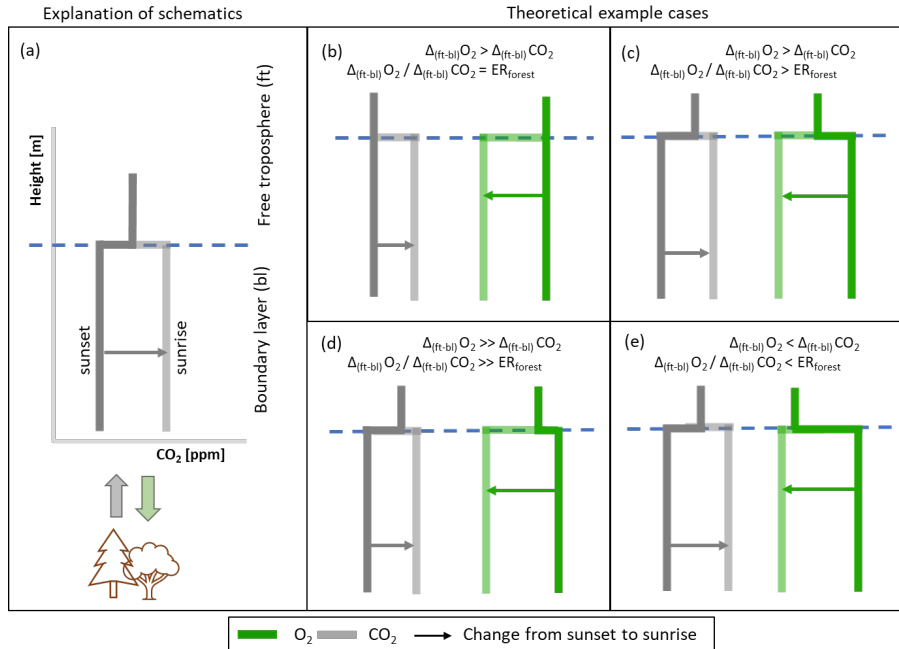


**Figure 8.** A schematic overview of how different ratios of the jumps of O<sub>2</sub> ( $\Delta_{(ft-bl)}O_2$ ) and CO<sub>2</sub> ( $\Delta_{(ft-bl)}CO_2$ ) are formed in the nighttime and how the ratio relates to the Exchange Ratio of the forest ( $ER_{forest}$ ). Panel (a) gives an explanation of the schematics and the other panels show four possibilities of different jump ratios ( $\Delta_{(ft-bl)}O_2/\Delta_{(ft-bl)}CO_2$ ): (b) the jump ratio is equal to  $ER_{forest}$ , (c) the jump ratio is larger than  $ER_{forest}$ , (d) the jump ratio is much larger than  $ER_{forest}$ , (e) the jump ratio is smaller than  $ER_{forest}$ . The bold lines represent the vertical profile just after sunset and the shaded lines represent the vertical profile just before sunrise.

an increase in the difference between  $ER_{atmos}$  and  $ER_{forest}$  may be due to either a low  $\beta_{CO_2}$  or a change in the jump ( $\Delta_{(ft-bl)}$ )  
 485 ratio. If the cause is the former (low  $\beta_{CO_2}$ ), the  $ER_{atmos}$  signal during P3 should be closer to  $ER_{forest}$ . If the latter (a high jump ratio),  $ER_{atmos}$  should remain well above  $ER_{forest}$  in P3.

### 5.3 Different $\Delta_{(ft-bl)}$ ratios

Knowing the vertical profile of O<sub>2</sub> and CO<sub>2</sub> especially during sunrise is essential to gain a more comprehensive understanding  
 490 of the formation of different jump ratios ( $\Delta_{(ft-bl)}O_2 / \Delta_{(ft-bl)}CO_2$ ) and to better interpret the diurnal behavior of the  $ER_{atmos}$  signal. However, due to lack of observational data we cannot validate the vertical profile of O<sub>2</sub> and CO<sub>2</sub> and the jump ratios. We therefore strongly recommend that future measurement campaigns include vertical measurements of both species. This can for example be done by flask sampling from aircraft, as we have done in a recent campaign in the Netherlands, of which preliminary results confirm that the values we have used here are realistic. Previous studies have also measured vertical profiles  
 495 of O<sub>2</sub> and CO<sub>2</sub>, but they primarily focused on well-mixed profiles during daytime or profiles over the ocean (Morgan et al.,

2019; Stephens et al., 2021; Ishidoya et al., 2022b). Hence, careful consideration of the timing and location of the vertical measurements is important to advance our knowledge of the diurnal behaviour of  $ER_{\text{atmos}}$ .

In the absence of observational data, we show with hypothetical situations that various jump ratios become possible (Figure 8). Both the  $O_2$  and  $CO_2$  jumps are formed as a result of three processes; the mixed-layer value before sunset (2a), the surface flux during the night (1) and the free troposphere value with the lapse rate (3) (we assume the lapse rate to be  $0 \text{ mol m}^{-1}$  for  $CO_2$  and  $O_2$ ). Most cases indicate that  $\Delta_{(ft-bl)}O_2$  is larger than  $\Delta_{(ft-bl)}CO_2$  above a forest, primarily because  $ER_{\text{forest}}$  is higher than 1.0 during the night ( $ER_r > 1.0$ ) as was shown in previous studies (Ishidoya et al., 2013; Angert et al., 2015; Hilman et al., 2022). It is noteworthy that the movement of the mixed-layer values from (P2a) to (P2b) in Figure 8 differs from its depiction in Figure 2c, where the focus was primarily on the transition between sunrise and sunset. We ignore the effect of subsidence (caused by mesoscale or synoptic processes) on the jump evaluation in this analysis, because it is likely of less importance compared to the other three processes.

It is highly likely that the jump ratio between  $O_2$  and  $CO_2$  cannot be directly linked to a specific ER for a certain process because of the interplay between the three processes that form the  $O_2$  and a  $CO_2$  jump (Figure 8d). The likelihood of both  $\Delta_{(ft-bl)}O_2$  and  $\Delta_{(ft-bl)}CO_2$  being zero at the end of the day is low because the surface flux during the day would form a jump (Figure 8c). Additionally, it is possible that the  $\Delta_{(ft-bl)}O_2$  is smaller than  $\Delta_{(ft-bl)}CO_2$  at the end of the day (Figure 8d) due to the daytime  $ER_{\text{forest}}$  being smaller than 1.0. Consequently,  $O_2$  will exhibit a faster movement across the zero line, resulting in a significantly larger  $\Delta_{(ft-bl)}O_2/\Delta_{(ft-bl)}CO_2$  ratio compared to  $ER_r$ .

515

Decoupling between the free troposphere and the boundary layer can lead to a scenario in which  $\Delta_{(ft-bl)}CO_2$  becomes larger than  $\Delta_{(ft-bl)}O_2$  (Figure 8e). This can occur for example, when the influence of fossil fuel sources causes a decrease in the  $O_2$  mole fraction and an increase in the  $CO_2$  mole fraction in the free troposphere, but large surface fluxes from the forest prevent such changes from occurring in the boundary layer. The jump ratio in this case again cannot be attributed to a single process. Some studies have demonstrated that decoupling between the boundary layer and the free troposphere can occur, leading to different ER signals (Sturm et al., 2005; van der Laan et al., 2014).

520

#### 5.4 Comparison with other studies

To the best of our knowledge, no previous studies have reported such high deviations of  $ER_{\text{atmos}}$  from  $ER_{\text{forest}}$ , or  $ER_{\text{atmos}}$  values higher than 2 for above forest canopy measurements as we found in Faassen et al. (2023). Only Liu et al. (2023b) found a non-linear relationship between  $O_2$  and other tracers that was difficult to explain. While some differences between  $ER_{\text{atmos}}$  and  $ER_{\text{forest}}$  have been observed in previous studies, these differences typically fall within a range of 0.5 (Seibt et al., 2004; Ishidoya et al., 2015; Battle et al., 2019; Yan et al., 2023). A possible reason for these smaller differences could be that most studies do not focus on such detailed diurnal analyses of  $ER_{\text{atmos}}$  for specific days but rather aggregate data from multiple days,

530 which could mitigate the extreme effects of entrainment by combining various jump possibilities. However, even in the study by Stephens et al. (2007), in which measurements at different heights are shown, no discernible difference in the  $ER_{\text{atmos}}$  signal for various diurnal cycles was observed, a finding that contrasts with our own analysis. The height at which measurements are made also influences the resulting  $ER_{\text{atmos}}$  signal. Closer to the canopy, the influence of entrainment is lower and  $ER_{\text{atmos}}$  is closer to  $ER_{\text{forest}}$  compared to measurements further away from the canopy (Faassen et al., 2023). However, we still found a  
535 high  $ER_{\text{atmos}}$  value of 2.28, even at a level just above the canopy (Faassen et al., 2023). Large values for  $ER_{\text{atmos}}$  have only been found at high latitude measurement stations (Sturm et al., 2005), due to the influence of the ocean.

There are several possibilities that could explain a constant  $ER_{\text{atmos}}$  signal during the day, which are not shown in our study. One possibility is that entrainment dominates throughout the day, caused by high jumps. If both the  $O_2$  and  $CO_2$  jumps are  
540 extremely high while the surface flux remains low, the  $ER_{\text{atmos}}$  value reflects the ratios between the jumps. In this scenario,  $ER_{\text{atmos}}$  cannot be used as an accurate indicator for the surface processes. Another explanation could be that the  $ER_{\text{forest}}$  signal is exactly 1.0 and entrainment is relatively low. When  $ER_{\text{forest}}$  equals 1.0, the diurnal cycle of the jumps would respond similarly. Together with a low entrainment flux (resulting from low jumps), it could lead to a constant  $ER_{\text{atmos}}$  value. Additionally, when the peak of  $ER_{\text{atmos}}$  occurs rapidly, there is a possibility that a low measurement precision would miss the extreme changes  
545 of  $ER_{\text{atmos}}$ . However, even in such cases,  $ER_{\text{atmos}}$  would still be influenced by entrainment, although its impact may be less discernible. It is crucial to note that in all these cases,  $ER_{\text{atmos}}$  remains influenced by entrainment to varying degrees.

Our study provides evidence that  $ER_{\text{atmos}}$  is almost always influenced by large scale processes and their diurnal variability, specifically entrainment, making it important to exercise caution when using it as an indicator for the surface ER processes.  
550 Instances where  $ER_{\text{atmos}}$  remains constant throughout daytime and serves as a reliable indication for  $ER_{\text{forest}}$  are likely rare. In comparison to previous studies (Seibt et al., 2004; Stephens et al., 2007; Ishidoya et al., 2013; Battle et al., 2019), it is unclear why Faassen et al. (2023) yields such extreme values for  $ER_{\text{atmos}}$  while the other studies do not show this, even though our modelling study here confirms the extreme  $ER_{\text{atmos}}$  values. Therefore, we recommend conducting more studies or performing detailed analyses of existing  $O_2$  and  $CO_2$  data sets to gain a better understanding of how changes in  $ER_{\text{atmos}}$  vary with time and  
555 space.

## 5.5 Comparison with other multi-tracer analyses

The impact of changes in large scale conditions such as entrainment on multi-tracer analyses above forest canopies extends beyond atmospheric  $O_2$ , encompassing other carbon cycle tracers such as carbon and oxygen isotopes ( $\delta^{13}C$  and  $\delta^{18}O$ ) (Wehr  
560 et al., 2016), and carbonyl sulfide (COS) (Whelan et al., 2018). Caution is required when employing methods of determining ratios between two species (eg. leaf relative uptake for COS and the ratios between different isotopes) that rely solely on single-height measurements. However, the influence of entrainment on these ratios would be less extreme compared to the  $ER_{\text{atmos}}$  signal because both COS and isotopes move in the same direction as  $CO_2$  itself. This is different compared to  $O_2$ , which always

565 moves in the opposite direction compared to CO<sub>2</sub>. When both species that form the ratio move in the same direction, ratios of different processes could be averaged and a one height measurement is more readily interpretable. Nevertheless, entrainment would still cause the two compounds that form the ratio to behave differently. We therefore emphasize the need to separately analyze the composition of the signal for each compound when ratios are analyzed.

570 Furthermore, we demonstrate in this study the potential of using ER<sub>atmos</sub> as an indicator of the extent of large scale processes. Additional tracers can strengthen this approach. δ<sup>13</sup>C, δ<sup>18</sup>O and COS signals exhibit differences between the surface and the free troposphere. Similar to O<sub>2</sub>, the onset of entrainment causes these signals to mix, yielding insights into how large scale processes influence the carbon cycle above a canopy (Berkelhammer et al., 2014; Vilà-Guerau de Arellano et al., 2019). By combining various tracers for CO<sub>2</sub>, we can create a comprehensive picture of the effects of small scale and large scale processes that influence carbon exchange.

## 575 6 Conclusions

We used a mixed-layer model to analyze the diurnal behavior of two Exchange Ratio (ER = O<sub>2</sub>/CO<sub>2</sub>) signals above a forest canopy: the ER of the atmosphere (ER<sub>atmos</sub> determined from the change over time of O<sub>2</sub> and CO<sub>2</sub> mole fraction measurements at a single height above the canopy) and the ER of the forest (ER<sub>forest</sub> determined from O<sub>2</sub> and CO<sub>2</sub> fluxes derived from the vertical gradient observations at two levels). We disentangled the biophysical processes influencing ER<sub>atmos</sub> to interpret single height O<sub>2</sub> and CO<sub>2</sub> measurements and to evaluate how both ER<sub>atmos</sub> and ER<sub>forest</sub> can be used to constrain carbon exchange above the canopy. The analysis is supported by the derivation of a new theoretical relationship that connects ER<sub>atmos</sub> and ER<sub>forest</sub> and by the use of a mixed-layer model that reproduces the O<sub>2</sub> and CO<sub>2</sub> diurnal cycles coupled to the dynamics of the atmospheric boundary layer. By combining the model with observations in a boreal forest during two contrasting summers of 2018 and 2019, we found three regimes during the day for ER<sub>atmos</sub>.

585

We find that the entrainment of air from the free troposphere leads to a diurnal cycle in ER<sub>atmos</sub>, resulting in three distinctive regimes: P1 at the start of the day, when the boundary layer has not yet started to grow, P2 when entrainment of air from the free troposphere into the boundary layer is dominant, and P3 at the end of the afternoon when entrainment becomes negligible. ER<sub>atmos</sub> can exhibit high values during P2 that cannot be attributed to an ER signal from a single process. During P3, ER<sub>atmos</sub> becomes closer to ER<sub>forest</sub>, and is therefore more representative for the forest exchange.

The large diurnal variability in ER<sub>atmos</sub> shows that single height O<sub>2</sub> and CO<sub>2</sub> measurements are insufficient to be used as an indication for the O<sub>2</sub>/CO<sub>2</sub> ratios of forest exchange. Our theoretical relationship between ER<sub>atmos</sub> and ER<sub>forest</sub> and model results show that the large diurnal variability is a result of the different behaviour of the O<sub>2</sub> and CO<sub>2</sub> diurnal cycle, which results in ER<sub>atmos</sub> values that cannot be attributed to a single process. To estimate the ER signal of the surface fluxes from above canopy measurements, ER<sub>forest</sub> should be used and therefore O<sub>2</sub> and CO<sub>2</sub> signals need to be measured at at least two heights, to allow

595

fluxes to be calculated from the vertical gradient. A single measurement height of O<sub>2</sub> and CO<sub>2</sub> could still be used to indicate the presence of advection of other carbon sources. However, the resulting ER<sub>atmos</sub> signal should be analysed with care, by taking into account the diurnal variability and the fact that the resulting ER is not necessarily the average of the individually  
600 ER signals of the contributing processes.

When O<sub>2</sub> and CO<sub>2</sub> measurements are available from 2 heights, the relationship between ER<sub>atmos</sub> and ER<sub>forest</sub> during P2 and P3 could provide valuable information about the changes in large-scale carbon processes (e.g. entrainment) and their influence on the smaller scale processes of the surface. A discrepancy between ER<sub>atmos</sub> and ER<sub>forest</sub> shows that large scale processes  
605 occur together with small scale processes at the surface. The difference between ER<sub>atmos</sub> and ER<sub>forest</sub> should be analysed with care as the size of the difference is not a direct indication of the size of the influence of the large scale processes. Differences between ER<sub>forest</sub> and ER<sub>atmos</sub> could be caused by several factors: changes in the size of the entrainment flux, the net surface flux or the difference between the free troposphere and the boundary layer (the 'jump') for O<sub>2</sub> and/or CO<sub>2</sub>, or changes in the jump ratio between O<sub>2</sub> and CO<sub>2</sub>.

610

In conclusion, single height O<sub>2</sub> and CO<sub>2</sub> measurements need to be analyzed with care, accounting for their dependence on canopy processes (represented by ER<sub>forest</sub>), but also for their capacity to integrate large scale processes resulting in values that cannot be attributed to a single process. To represent the forest exchange, the ER<sub>forest</sub> signal based on measurements at at least two heights should be used instead.

615

*Code availability.* The data used in this study are available from <https://doi.org/10.18160/SJ3J-PD38> (Faassen and Luijkx, 2022). The model code for the CLASS model can be found in <https://classmodel.github.io/>

## Appendix A: Appendix

### A1 Evaluation of the theoretical relationship between ER<sub>atmos</sub> and ER<sub>forest</sub>

620 In this Section, we analyze Equation 8 to explore the response of ER<sub>atmos</sub> to changes in the variables in this equation and to investigate when ER<sub>atmos</sub> aligns with ER<sub>forest</sub> and thereby accurately reflects local processes. Based on Equation 8, the ER<sub>atmos</sub> signal equals ER<sub>forest</sub> when the  $\beta$  values of O<sub>2</sub> and CO<sub>2</sub> are equal. We can define four different regimes where the  $\beta$  values change significantly. As depicted in Figure 1 we can define two regimes based on the entrainment velocity: an entrainment driven (left panels in Figure A1) and a photosynthesis driven regime right panels in Figure A1). To complete the analysis we  
625 considered two distinct cases for the jump of O<sub>2</sub> (top versus bottom panels).



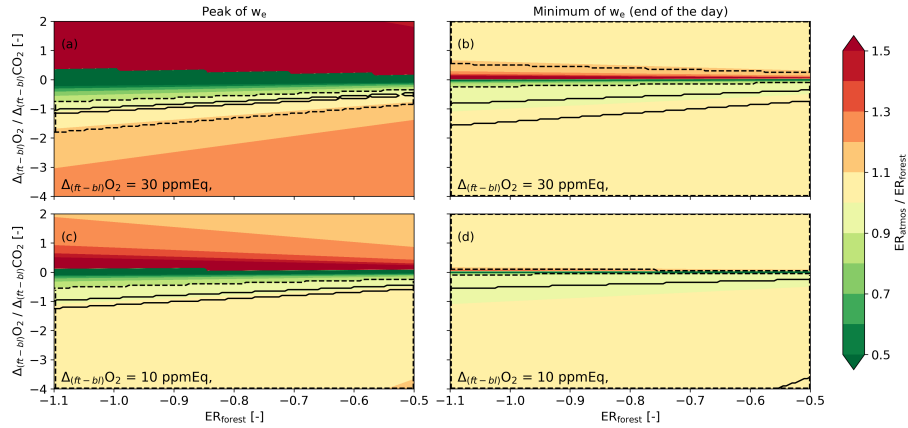


**Figure A1.** Analysis of Equation 8 for the entrainment- and photosynthesis-driven regimes. The ratio between  $ER_{\text{forest}}$  and  $ER_{\text{atmos}}$  is evaluated based on changes in  $ER_{\text{forest}}$  and the ratio of the jumps of  $O_2$  and  $CO_2$  between the free troposphere and the boundary layer ( $\Delta_{(ft-bl)}$ ) for 4 cases: with a high entrainment velocity ( $w_e = 0.10 \text{ m s}^{-1}$ ) (left panels) and a low entrainment velocity ( $w_e = 0.01 \text{ m s}^{-1}$ ) (right panels) and for situations with a high  $O_2$  jump ( $\Delta_{(ft-bl)}O_2 = 0.30 \text{ ppmEq}$ ) (top panels) and a low  $O_2$  jump ( $\Delta_{(ft-bl)}O_2 = 0.10 \text{ ppmEq}$ ) (bottom panels). The  $O_2$  surface flux  $F(O_2)_s$  is kept constant for all the panels, at  $8.5 \mu\text{mol m}^{-1} \text{ s}^{-1}$ .

Based on Equation 8 we systematically varied  $\Delta_{(ft-bl)}CO_2$  and  $(F_{CO_2})_s$  over plausible ranges and kept the other variables constant. As a result we derived  $ER_{\text{forest}} \cdot ER_{\text{atmos}}$  ratios for these four regimes, where a value of 1.0 now indicates that  $ER_{\text{atmos}}$  is equal to  $ER_{\text{forest}}$ . The selected values and ranges for the four different cases were informed by initial conditions from the  
630 Hyytiälä case, studied in Faassen et al. (2023) and the corresponding model simulations presented in Section 3.2.4.

There are a few situations where the  $\beta$  values of  $O_2$  and  $CO_2$  are equal and these are indicated in Figure A1 as the area between the black solid lines ( $ER_{\text{atmos}}$  deviates  $<1\%$  from  $ER_{\text{forest}}$ ) and dashed lines ( $ER_{\text{atmos}}$  deviates  $<10\%$  from  $ER_{\text{forest}}$ ):

1. During the photosynthesis dominant regime. When the entrainment velocity ( $w_e$ ) is close to zero, both  $\beta$  values become  
635 zero. This is likely at the end of the day (right panels in Figure 1).
2. When the  $\beta$  values for  $O_2$  and  $CO_2$  become equal which happens when  $\Delta_{(ft-bl)}O_2 / \Delta_{(ft-bl)}CO_2 = ER_{\text{forest}}$ . A specific case is when the  $\Delta_{(ft-bl)}O_2 = \Delta_{(ft-bl)}CO_2$ . In that case, the  $ER_{\text{forest}}$  has to be 1.0 for the  $\beta$  values of  $O_2$  and  $CO_2$  to become equal. The  $\beta$  values of  $O_2$  and  $CO_2$  are become closer during the lower  $O_2$  jump case (lower panels in Figure 1).

The last situation only occurs under very specific conditions when the ratio of the  $O_2$  and  $CO_2$  entrainment and surface fluxes  
640 are the same. This is visible in the left panels of Figure A1, where only a small part of the graph shows values of  $ER_{\text{atmos}}$  close to  $ER_{\text{forest}}$  (indicated by the area between solid lines). In contrast, during low entrainment velocities at the end of the afternoon, it is more likely that the  $ER_{\text{atmos}}$  values become close to  $ER_{\text{forest}}$ , and this is shown by the larger area in the right panels of Figure A1. Low entrainment velocities could also occur when the growth of the boundary layer is reduces due to subsidence.

During this study we will not focus on this specific case.

645

There are also differences between  $ER_{\text{atmos}}$  and  $ER_{\text{forest}}$  that arise from variations in the  $\beta$  values. Figure A1 demonstrates that substantial differences between  $ER_{\text{atmos}}$  and  $ER_{\text{forest}}$  originate due to differences in the entrainment fluxes for both species. When  $\Delta_{(ft-bl)}O_2$  exceeds  $\Delta_{(ft-bl)}CO_2$ , this implies a dominant entrainment flux of  $O_2$  over  $CO_2$  and  $\beta_{O_2}$  deviates further from  $\beta_{CO_2}$  (Equation 8). This effect is almost absent when the jumps themselves are lower, because the  $ER_{\text{atmos}} / ER_{\text{forest}}$  ratio stays around 1 (Figure A1c). Moreover, when  $\Delta_{(ft-bl)}CO_2$  transitions from negative to positive, the sign of  $\beta_{CO_2}$  also changes, subsequently elevating the  $ER_{\text{atmos}}$  values (Equation 8).

$ER_{\text{atmos}}$  can also become smaller than  $ER_{\text{forest}}$  when  $\Delta_{(ft-bl)}CO_2$  is larger than  $\Delta_{(ft-bl)}O_2$  (Figure A1). This difference results in a large value for  $\beta_{CO_2}$  compared to  $\beta_{O_2}$ , causing the  $ER_{\text{forest}}$  value to be multiplied by a factor less than 1 and leading to a lower  $ER_{\text{atmos}}$  value than  $ER_{\text{forest}}$  (equation 8). By assessing  $ER_{\text{atmos}}$  and  $ER_{\text{forest}}$  values, we can see whether  $\Delta_{(ft-bl)}O_2$  exceeds  $\Delta_{(ft-bl)}CO_2$  ( $ER_{\text{atmos}} > ER_{\text{forest}}$ ) or vice versa ( $ER_{\text{atmos}} < ER_{\text{forest}}$ ).

This illustrative analysis, based on prescribed values in Equation 8 and Figure A1, provides an initial estimate of the variability in  $ER_{\text{atmos}}$ . However, it lacks insights into the diurnal behavior of the individual components of equation 8 and their potential combinations.

660

## A2 Implementation of $O_2$ in CLASS

The following equation shows the implementation of the tendency (change over time) of  $O_2$  into CLASS:

$$\frac{dO_2}{dt} = \frac{F_{O_2(s)} - F_{O_2(e)}}{h} + adv_{O_2} \quad (A1)$$

where  $F_{O_2(s)}$  is the net surface  $O_2$  flux at the canopy,  $F_{O_2(e)}$  is the  $O_2$  entrainment flux,  $h$  is the boundary layer height and  $adv_{O_2}$  is the advection term. The surface flux is calculated with equation 10 and the entrainment flux is based on the following equation (see also equation 2):

$$F_{O_2(e)} = -w_e \cdot \Delta_{(ft-bl)}O_2 \quad (A2)$$

where  $w_e$  is the entrainment velocity and  $\Delta_{(ft-bl)}O_2$  is the jump of  $O_2$ . The jump of  $O_2$  was determined the same way as for  $CO_2$ , by tuning the jump until the decrease/increase in  $CO_2/O_2$  matched during the entrainment dominant period.

670

## A3 Validation of CLASS

Figures A3 and A2 present a comparison between the model output of CLASS and the corresponding measurements for the representative days of 2018 and 2019, assessing various parameters. Both figures demonstrate that the model compares well

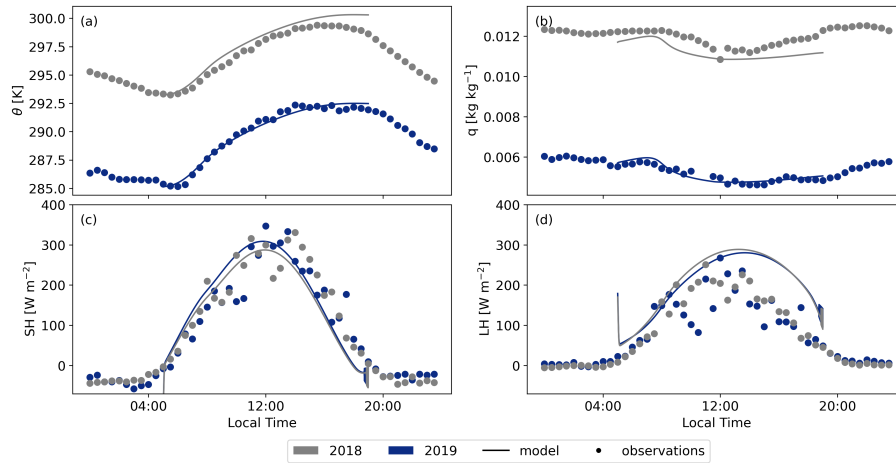


**Figure A2.** Comparison between the 2019 and 2018 case modelled with CLASS with the observational data for the potential temperature ( $\theta$ ) (a), specific humidity ( $q$ ) (b), Sensible heat flux (SH) (c), Latent heat flux (LH) (d).

675 to the observed data. CLASS accurately follows the observed temperature increase (Figure A2a). A constant difference of approximately 8K between 2018 and 2019 is seen for both model and observations. This persistent difference is attributed to a heat wave rather than a drought in Hyytiälä, as a drought would have intensified the divergence between the 2018 and 2019 simulations throughout the day. Moreover, CLASS adequately models specific humidity for both years, assuming an initial relative humidity of 80% for 2018 (Figure A2b). The sensible heat flux (Figure A2c) and latent heat (Figure A2d) exhibit  
 680 minimal differences between the 2018 and 2019 simulations. The accurate representation of atmospheric properties in CLASS consequently results in a satisfactory comparison of the boundary layer height development for both years in comparison to the observed data from radiosondes (Figure A3a)

The various CO<sub>2</sub> fluxes simulated by CLASS exhibit a high level of agreement with the observational data for both 2018  
 685 and 2019 (Figure A3d and A3e). While there are subtle differences evident between the observations for the two years, CLASS adeptly captures these nuances. Consequently, the model provides an accurate representation of plant behavior under both normal and warmer conditions. The elevated temperatures (+8K) and slightly reduced soil moisture (-0.03 m<sup>3</sup> m<sup>-3</sup>) contribute to a slightly higher GPP and TER flux. Our study reaffirms that the vegetation in Hyytiälä did not undergo any stress during the 2018 European drought, which would have resulted in a lower GPP and lower latent heat flux (Lindroth et al., 2020).

690

For the 2018 case, we only altered a few initial conditions (see Table C3). However, both the decrease in CO<sub>2</sub> and the increase in O<sub>2</sub> during the day exhibit close similarity between the model and the observations. This outcome underscores that even with minimal changes in the initial conditions for the 2018 case and keeping the other variables constant (e.g., the jumps),

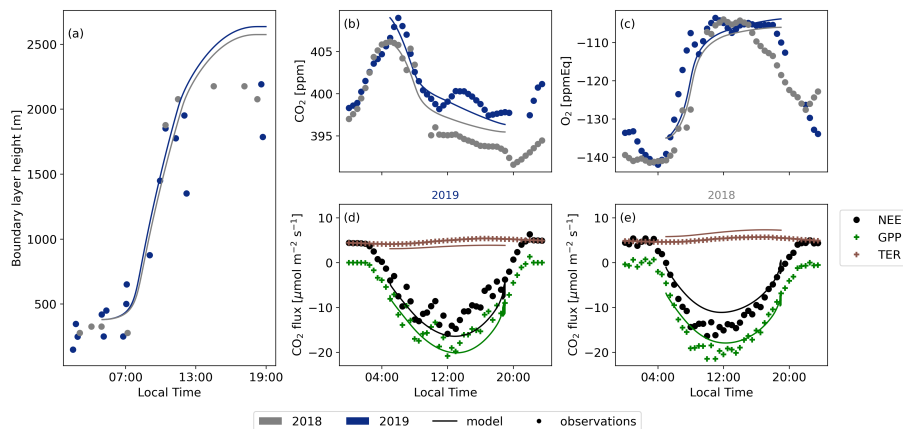


**Figure A3.** Comparison between the 2019 and 2018 case modelled with CLASS with the observational data for the boundary layer height (a), CO<sub>2</sub> (b), O<sub>2</sub> (c), the 2019 CO<sub>2</sub> surface fluxes (d) and the 2018 CO<sub>2</sub> surface fluxes (e).

we can successfully replicate a realistic new day based on the base case.

695

It is important to note that only the Net Ecosystem Exchange (NEE) data are obtained directly from Eddy Covariance measurements. The Gross Primary Production (GPP) is inferred from a light and temperature based function and the total ecosystem respiration is calculated as the residual between NEE and GPP (Kulmala et al., 2019; Kohonen et al., 2022). This distinction may explain the challenge in aligning the TER flux of the observations with the model, as the model exhibits notable discrepancies from the observations for both the 2018 and 2019 cases. The model's simulated respiration increase based on temperature appears more extreme compared to the observations. However, several studies (Lindroth et al., 2008; Gao et al., 2017; Heiskanen et al., 2023) indicate that the model's increase in TER between 2018 and 2019 is slightly too high, while the change based on observations is too low. As a result, it is plausible that the true respiration flux lies somewhere between the model output and the observational data.

705

## Appendix B: Figures

## Appendix C: Tables

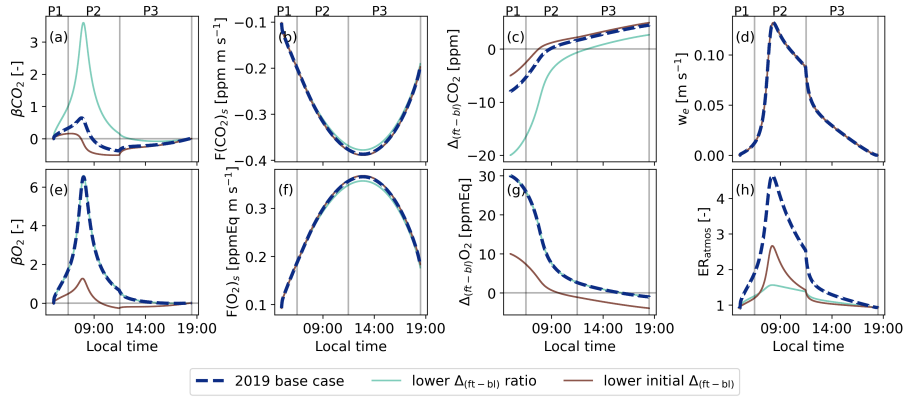


**Figure B1.** Similar to Figure 5 but now for the base case (2019) and the background sensitivity studies with a lower jump ratio between  $O_2$  and  $CO_2$  (lower  $\Delta_{(ft-bl)}$ ) and with a lower initial jump for  $CO_2$  (lower initial  $\Delta_{(ft-bl)}$ ). The diurnal variability of the exchange ratio of the atmosphere is now added ( $ER_{atmos}$ : (h))

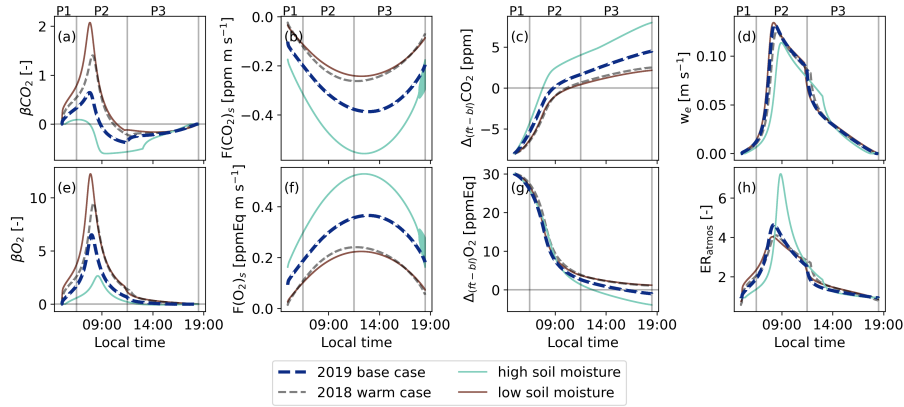


**Figure B2.** Similar to Figure 5 but now for the base case (2019) and the dry and warm sensitivity studies with a high soil moisture and a low soil moisture, both with higher air temperatures compared to the 2019 base case. The diurnal variability of the exchange ratio of the atmosphere is now added ( $ER_{atmos}$ : (h))

**Table C1.** The initial conditions used for the three sensitivity analyses, compared to the initial conditions for the 2019 base case. The subscript (0) indicates the first time step.

Variable	2019 base	background air		climate	
		lower $\Delta_{(ft-bl)}$ ratio	lower initial $\Delta_{(ft-bl)}$	high SMI	low SMI
$\Delta_{(ft-bl)}O_{2(0)}$ [ppmEq]	30	30	10	2019 case	2019 case
$\Delta_{(ft-bl)}CO_{2(0)}$ [ppm]	-8	-20	-5	2019 case	2019 case
$\theta_0$ [K]	285.2	2019 case	2019 case	290	290
Soil moisture [ $m^3 m^{-3}$ ]	0.18	2019 case	2019 case	0.22	0.14

**Table C2.** Initialisation of the CLASS model for the base case of 2019, based on 10-07-2019. The initialisation is based on the SMEAR II data (Hari et al., 2013), our OXHYYGEN campaign data (radiosondes or O<sub>2</sub> and CO<sub>2</sub> measurements) (Faassen et al., 2023) and studies that show ranges for parameters for the plants and soil (Lindroth et al., 2008; ECMWF IV, 2014; Vilà-Guerau de Arellano et al., 2015) .

Parameter [Source]	Description	Initial value
Lat	Latitude [deg]	61.51
Lon	Longitude [deg]	24.17
DOY	Day of year [-]	191
t <sub>0</sub>	Starting time [UTC]	3
h <sub>1</sub>	Initial boundary layer height [m]	380
h <sub>2</sub>	Height of the residual layer [m]	2016
P	Surface pressure [hPa]	988.72
<i>Temperature:</i>		
θ <sub>0</sub>	Initial potential temperature [K]	285.15
Δθ <sub>0</sub>	Initial potential temperature jump [K]	2.4
λθ <sub>1</sub>	Potential temperature lapse rate of residual layer [K m <sup>-1</sup> ]	0.0023
λθ <sub>2</sub>	Potential temperature lapse rate of free troposphere [K m <sup>-1</sup> ]	0.0057
<i>Specific humidity:</i>		
q <sub>0</sub>	Initial specific humidity [kg kg <sup>-1</sup> ]	5.7 x 10 <sup>-3</sup>
Δq <sub>0</sub>	Initial specific humidity jump [kg kg <sup>-1</sup> ]	-1.2 x 10 <sup>-3</sup>
λq <sub>1</sub>	Specific humidity lapse rate of residual layer [kg kg <sup>-1</sup> m <sup>-1</sup> ]	-8.3 x 10 <sup>-7</sup>
λq <sub>2</sub>	Specific humidity lapse rate of free troposphere [kg kg <sup>-1</sup> m <sup>-1</sup> ]	-2.3 x 10 <sup>-6</sup>
<i>Carbon:</i>		
CO <sub>2,0</sub>	Initial CO <sub>2,0</sub> mole fraction [ppm]	409
ΔCO <sub>2,0</sub>	Initial CO <sub>2</sub> jump [ppm]	-8
λCO <sub>2</sub>	CO <sub>2</sub> lapse rate of free troposphere [ppm m <sup>-1</sup> ]	0
<i>Oxygen:</i>		
O <sub>2,0</sub>	Initial O <sub>2</sub> [ppm]	-135
ΔO <sub>2,0</sub>	Initial O <sub>2</sub> jump [ppm]	30
λO <sub>2</sub>	O <sub>2</sub> lapse rate of free troposphere [ppm m <sup>-1</sup> ]	0
<i>Vegetation:</i>		
LAI	Leaf Area Index [-]	3.3
C <sub>veg</sub>	Vegetation cover [-]	0.9
r <sub>e,min</sub>	Minimum resistance transpiration [s m <sup>-1</sup> ]	500
r <sub>s,soil,min</sub>	Minimum resistance soil evaporation [s m <sup>-1</sup> ]	250
g <sub>D</sub>	VPD correction factor for surface resistance [-]	0.03
z <sub>0,m</sub>	Roughness length for momentum [m]	2.0
z <sub>0,h</sub>	Roughness length for heat and moisture [m]	2.0
α	albedo [-]	0.10
R <sub>10</sub>	Respiration at 10 degrees [μg CO <sub>2</sub> m <sup>-2</sup> s <sup>-1</sup> ]	0.148
g <sub>m</sub>	Mesophyl conductance [mm s <sup>-1</sup> ]	2
T <sub>2gm</sub>	reference temperature to calculate g <sub>m</sub> [K]	305
C <sub>...</sub>	Curvature of response curve to drought [-]	0.15

**Table C3.** Adjustments for the 2018 case (warm case) compared to the 2019 values shown in in table C2. Only the initial potential temperature ( $\theta_0$ ), initial soil moisture ( $w_g$ ) and CO<sub>2</sub> mole fraction (CO<sub>2,0</sub>) are adjusted based on the aggregate of 28-07-2018 and 29-07-2018. It was assumed that the initial relative humidity stayed constant at 80% with increasing temperatures, therefore the initial specific humidity was also adjusted.

Parameter	Description	Initial value
$\theta_0$	Initial potential temperature [K]	293.3
$T_{\text{soil},1}$	Initial top soil temperature [K]	$\theta_0 - 2$
$T_{\text{soil},2}$	Initial deeper soil temperature [K]	$\theta_0 - 3$
$q_0$	Initial specific humidity [ $\text{kg kg}^{-1}$ ]	$f(\theta_0)$
$w_g$	Volumetric water content of top soil layer [ $\text{m}^3 \text{m}^{-3}$ ]	$w_2 - 0.04$
$w_2$	Volumetric water content of deeper soil layer [ $\text{m}^3 \text{m}^{-3}$ ]	0.15
CO <sub>2,0</sub>	Initial CO <sub>2</sub> mole fraction [ppm]	406

*Author contributions.* KAPF, JV, ITL and RG-A set up the model analysis. KAPF, ITL, JV and WP interpreted and discussed the methods and results. ITL designed the measurement campaign and conducted the O<sub>2</sub> and CO<sub>2</sub> measurements, and BGH conducted the radiosonde measurements with input from JV and support from IM. KAPF and ITL wrote the manuscript with input from all co-authors.

*Competing interests.* There are no competing interests.

*Acknowledgements.* The authors would like to thank the following persons for their help during the measurement campaigns at Hyytiälä in 2018 and 2019: Janne Levula (previously at Institute for Atmospheric and Earth System Research (INAR) / Physics, Faculty of Science, University of Helsinki, Helsinki, Finland), Timo Vesala (Institute for Atmospheric and Earth System Research (INAR) / Physics, Faculty of Science, University of Helsinki, Helsinki, Finland), Linh N.T. Nguyen (previously at University of Groningen, Centre for Isotope Research, Energy and Sustainability Research Institute Groningen, Groningen, the Netherlands), Bert Kers (University of Groningen, Centre for Isotope Research, Energy and Sustainability Research Institute Groningen, Groningen, the Netherlands) and Brian Verhoeven (former student at Meteorology and Air Quality, Wageningen University, Wageningen, the Netherlands). We acknowledge Ruben van 't Loo (student Meteorology and Air Quality, Wageningen University, Wageningen, the Netherlands) for his contribution to the data analysis. We have used ChatGPT as a language editor to improve the readability of certain parts of the manuscript. This work was supported with funding from the Netherlands Organisation for Scientific Research for ITL (016.Veni.171.095 and VI.Vidi.213.143). The measurements at Hyytiälä are supported by the University of Helsinki via ICOS-HY funding and the GreenFeedBack project from the EU Horizon Europe – Framework Programme for Research and Innovation (no. 101056921).



## References

- 725 Angert, A., Yakir, D., Rodeghiero, M., Preisler, Y., Davidson, E. A., and Weiner, T.: Using O<sub>2</sub> to study the relationships between soil CO<sub>2</sub> efflux and soil respiration, *Biogeosciences*, 12, 2089–2099, <https://doi.org/10.5194/bg-12-2089-2015>, 2015.
- Battle, M. O., William Munger, J., Conley, M., Sofen, E., Perry, R., Hart, R., Davis, Z., Scheckman, J., Woogerd, J., Graeter, K., Seekins, S., David, S., and Carpenter, J.: Atmospheric measurements of the terrestrial O<sub>2</sub> : CO<sub>2</sub> exchange ratio of a midlatitude forest, *Atmospheric Chemistry and Physics*, 19, 8687–8701, <https://doi.org/10.5194/acp-19-8687-2019>, 2019.
- 730 Berkelhammer, M., Asaf, D., Still, C., Montzka, S., Noone, D., Gupta, M., Provencal, R., Chen, H., and Yakir, D.: Constraining surface carbon fluxes using in situ measurements of carbonyl sulfide and carbon dioxide, *Global Biogeochemical Cycles*, 28, 161–179, 2014.
- Bloom, A. J.: Photorespiration and nitrate assimilation: a major intersection between plant carbon and nitrogen, *Photosynthesis research*, 123, 117–128, 2015.
- Casso-Torralba, P., Vilà-Guerau de Arellano, J., Bosveld, F., Soler, M. R., Vermeulen, A., Werner, C., and Moors, E.: Diurnal and vertical variability of the sensible heat and carbon dioxide budgets in the atmospheric surface layer, *Journal of Geophysical Research: Atmospheres*, 113, 2008.
- 735 Combe, M., Vilà-Guerau de Arellano, J., Ouwersloot, H. G., Jacobs, C. M., and Peters, W.: Two perspectives on the coupled carbon, water and energy exchange in the planetary boundary layer, *Biogeosciences*, 12, 103–123, 2015.
- ECMWF IV, I.: Documentation—Cy40r1 Part IV: Physical Processes, European Centre for Medium-Range Weather Forecasts: Reading, 740 UK, 2014.
- Faassen, K. and Lujikx, I.: Atmospheric O<sub>2</sub> and CO<sub>2</sub> measurements at Hyytiälä, Finland, <https://doi.org/10.18160/SJ3J-PD38>, last accessed: 06-01-2023, 2022.
- Faassen, K. A., Nguyen, L. N., Broekema, E. R., Kers, B. A., Mammarella, I., Vesala, T., Pickers, P. A., Manning, A. C., Vilà-Guerau de Arellano, J., Meijer, H. A., et al.: Diurnal variability of atmospheric O<sub>2</sub>, CO<sub>2</sub>, and their exchange ratio above a boreal forest in southern 745 Finland, *Atmospheric Chemistry and Physics*, 23, 851–876, 2023.
- Fischer, S., Hanf, S., Frosch, T., Gleixner, G., Popp, J., Trumbore, S., and Hartmann, H.: *Pinus sylvestris* switches respiration substrates under shading but not during drought, *New Phytologist*, 207, 542–550, 2015.
- Friedlingstein, P., Jones, M. W., O’Sullivan, M., Andrew, R. M., Bakker, D. C., Hauck, J., Le Quéré, C., Peters, G. P., Peters, W., Pongratz, J., et al.: Global carbon budget 2021, *Earth System Science Data*, 14, 1917–2005, 2022.
- 750 Gao, Y., Markkanen, T., Aurela, M., Mammarella, I., Thum, T., Tsuruta, A., Yang, H., and Aalto, T.: Response of water use efficiency to summer drought in a boreal Scots pine forest in Finland, *Biogeosciences*, 14, 4409–4422, 2017.
- Gibelin, A.-L., Calvet, J.-C., and Viovy, N.: Modelling energy and CO<sub>2</sub> fluxes with an interactive vegetation land surface model-Evaluation at high and middle latitudes, *Agricultural and forest meteorology*, 148, 1611–1628, 2008.
- Hari, P., Nikinmaa, E., Pohja, T., Siivola, E., Bäck, J., Vesala, T., and Kulmala, M.: Station for measuring ecosystem-atmosphere relations: 755 SMEAR, in: *Physical and physiological forest ecology*, pp. 471–487, Springer, 2013.
- Heiskanen, L., Tuovinen, J.-P., Vekuri, H., Räsänen, A., Virtanen, T., Juutinen, S., Lohila, A., Mikola, J., and Aurela, M.: Meteorological responses of carbon dioxide and methane fluxes in the terrestrial and aquatic ecosystems of a subarctic landscape, *Biogeosciences*, 20, 545–572, 2023.
- Hilman, B. and Angert, A.: Measuring the ratio of CO<sub>2</sub> efflux to O<sub>2</sub> influx in tree stem respiration, *Tree Physiology*, 36, 1422–1431, 2016.

- 760 Hilman, B., Weiner, T., Haran, T., Masiello, C. A., Gao, X., and Angert, A.: The apparent respiratory quotient of soils and tree stems and the processes that control it, *Journal of Geophysical Research: Biogeosciences*, 127, e2021JG006676, 2022.
- Ishidoya, S., Murayama, S., Takamura, C., Kondo, H., Saigusa, N., Goto, D., Morimoto, S., Aoki, N., Aoki, S., and Nakazawa, T.: O<sub>2</sub>:CO<sub>2</sub> exchange ratios observed in a cool temperate deciduous forest ecosystem of central Japan, *Tellus B: Chemical and Physical Meteorology*, 65, 211–220, <https://doi.org/10.3402/tellusb.v65i0.21120>, 2013.
- 765 Ishidoya, S., Murayama, S., Kondo, H., Saigusa, N., Kishimoto-Mo, A. W., and Yamamoto, S.: Observation of O<sub>2</sub>:CO<sub>2</sub> exchange ratio for net turbulent fluxes and its application to forest carbon cycles, *Ecological Research*, 30, 225–234, <https://doi.org/10.1007/s11284-014-1241-3>, 2015.
- Ishidoya, S., Sugawara, H., Terao, Y., Kaneyasu, N., Aoki, N., Tsuboi, K., and Kondo, H.: O<sub>2</sub>:CO<sub>2</sub> exchange ratio for net turbulent flux observed in an urban area of Tokyo, Japan, and its application to an evaluation of anthropogenic CO<sub>2</sub> emissions, *Atmospheric Chemistry and Physics*, 20, 5293–5308, 2020.
- 770 Ishidoya, S., Tsuboi, K., Kondo, H., Ishijima, K., Aoki, N., Matsueda, H., and Saito, K.: Measurement report: Method for evaluating CO<sub>2</sub> emission from a cement plant by atmosphere O<sub>2</sub>/N<sub>2</sub> and CO<sub>2</sub> measurements and its applicability to the detection of CO<sub>2</sub> capture signals, *Atmospheric Chemistry and Physics Discussions*, pp. 1–26, 2022a.
- Ishidoya, S., Tsuboi, K., Niwa, Y., Matsueda, H., Murayama, S., Ishijima, K., and Saito, K.: Spatiotemporal variations of the  $\delta$  (O<sub>2</sub>/N<sub>2</sub>), CO<sub>2</sub> and  $\delta$  (APO) in the troposphere over the western North Pacific, *Atmospheric Chemistry and Physics*, 22, 6953–6970, 2022b.
- 775 Jacobs, C., Van den Hurk, B., and De Bruin, H.: Stomatal behaviour and photosynthetic rate of unstressed grapevines in semi-arid conditions, *Agricultural and Forest Meteorology*, 80, 111–134, 1996.
- Kaimal, J. C. and Finnigan, J. J.: *Atmospheric boundary layer flows: their structure and measurement*, Oxford university press, 1994.
- Keeling, R. F. and Manning, A. C.: *Studies of Recent Changes in Atmospheric O<sub>2</sub> Content*, vol. 5, Elsevier Ltd., 2 edn., <https://doi.org/10.1016/B978-0-08-095975-7.00420-4>, 2014.
- 780 Keeling, R. F., Manning, A. C., McEvoy, E. M., and Shertz, S. R.: Methods for measuring changes in atmospheric O<sub>2</sub> concentration and their application in southern hemisphere air, *Journal of Geophysical Research: Atmospheres*, 103, 3381–3397, 1998.
- Kohonen, K.-M., Dewar, R., Tramontana, G., Mauranen, A., Kolari, P., Kooijmans, L. M., Papale, D., Vesala, T., and Mammarella, I.: Intercomparison of methods to estimate gross primary production based on CO<sub>2</sub> and COS flux measurements, *Biogeosciences*, 19, 4067–4088, 2022.
- 785 Kulmala, L., Pumpanen, J., Kolari, P., Dengel, S., Berninger, F., Köster, K., Matkala, L., Vanhatalo, A., Vesala, T., and Bäck, J.: Inter- and intra-annual dynamics of photosynthesis differ between forest floor vegetation and tree canopy in a subarctic Scots pine stand, *Agricultural and Forest Meteorology*, 271, 1–11, 2019.
- Lilly, D. K.: Models of cloud-topped mixed layers under a strong inversion, *Quarterly Journal of the Royal Meteorological Society*, 94, 292–309, 1968.
- 790 Lindroth, A., Lagergren, F., Aurela, M., Bjarnadottir, B., Christensen, T., Dellwik, E., Grelle, A., Ibrom, A., Johansson, T., Lankreijer, H., et al.: Leaf area index is the principal scaling parameter for both gross photosynthesis and ecosystem respiration of Northern deciduous and coniferous forests, *Tellus B: Chemical and Physical Meteorology*, 60, 129–142, 2008.
- Lindroth, A., Holst, J., Linderson, M.-L., Aurela, M., Biermann, T., Heliasz, M., Chi, J., Ibrom, A., Kolari, P., Klemmedtsson, L., et al.: Effects of drought and meteorological forcing on carbon and water fluxes in Nordic forests during the dry summer of 2018, *Philosophical Transactions of the Royal Society B*, 375, 20190516, 2020.
- 795

- Liu, X., Huang, J., Wang, L., Lian, X., Li, C., Ding, L., Wei, Y., Chen, S., Wang, Y., Li, S., et al.: “Urban Respiration” Revealed by Atmospheric O<sub>2</sub> Measurements in an Industrial Metropolis, *Environmental Science & Technology*, 57, 2286–2296, 2023a.
- 800 Liu, X., Wang, L., Huang, J., Wang, Y., Li, C., Ding, L., Lian, X., and Shi, J.: Revealing the Covariation of Atmospheric O<sub>2</sub> and Pollutants in an Industrial Metropolis by Explainable Machine Learning, *Environmental Science & Technology Letters*, 2023b.
- Manning, A. C. and Keeling, R. F.: Global oceanic and land biotic carbon sinks from the scripps atmospheric oxygen flask sampling network, *Tellus, Series B: Chemical and Physical Meteorology*, 58, 95–116, <https://doi.org/10.1111/j.1600-0889.2006.00175.x>, 2006.
- Miller, J. B. and Tans, P. P.: Calculating isotopic fractionation from atmospheric measurements at various scales, *Tellus B: Chemical and Physical Meteorology*, 55, 207–214, 2003.
- 805 Morgan, E. J., Stephens, B. B., Long, M. C., Keeling, R. F., Bent, J. D., McKain, K., Sweeney, C., Hoecker-Martínez, M. S., and Kort, E. A.: Summertime Atmospheric Boundary Layer Gradients of O<sub>2</sub> and CO<sub>2</sub> over the Southern Ocean, *Journal of Geophysical Research: Atmospheres*, 124, 13 439–13 456, 2019.
- Ouwensloot, H., Vilà-Guerau de Arellano, J., Nölscher, A., Krol, M., Ganzeveld, L., Breitenberger, C., Mammarella, I., Williams, J., and Lelieveld, J.: Characterization of a boreal convective boundary layer and its impact on atmospheric chemistry during HUMPPA-COPEC-810 2010, *Atmospheric Chemistry and Physics*, 12, 9335–9353, 2012.
- Peters, W., Bastos, A., Ciais, P., and Vermeulen, A.: A historical, geographical and ecological perspective on the 2018 European summer drought, *Philosophical transactions of the royal society B*, 375, 20190 505, 2020.
- Pickers, P. A., Manning, A. C., Le Quéré, C., Forster, G. L., Luijkx, I. T., Gerbig, C., Fleming, L. S., and Sturges, W. T.: Novel quantification of regional fossil fuel CO<sub>2</sub> reductions during COVID-19 lockdowns using atmospheric oxygen measurements, *Science advances*, 8, 815 eabl9250, 2022.
- Reichstein, M., Falge, E., Baldocchi, D., Papale, D., Aubinet, M., Berbigier, P., Bernhofer, C., Buchmann, N., Gilmanov, T., Granier, A., et al.: On the separation of net ecosystem exchange into assimilation and ecosystem respiration: review and improved algorithm, *Global change biology*, 11, 1424–1439, 2005.
- Rödenbeck, C., Le Quéré, C., Heimann, M., and Keeling, R. F.: Interannual variability in oceanic biogeochemical processes inferred by inversion of atmospheric O<sub>2</sub>/N<sub>2</sub> and CO<sub>2</sub> data, *Tellus, Series B: Chemical and Physical Meteorology*, 60 B, 685–705, <https://doi.org/10.1111/j.1600-0889.2008.00375.x>, 2008.
- 820 Rödenbeck, C., Adcock, K. E., Eritt, M., Gachkivskyi, M., Gerbig, C., Hammer, S., Jordan, A., Keeling, R. F., Levin, I., Maier, F., et al.: The suitability of atmospheric oxygen measurements to constrain Western European fossil-fuel CO<sub>2</sub> emissions and their trends, 2023.
- Ronda, R., De Bruin, H., and Holtslag, A.: Representation of the canopy conductance in modeling the surface energy budget for low vegetation, *Journal of Applied Meteorology and Climatology*, 40, 1431–1444, 2001.
- 825 Schulte, R., van Zanten, M., Rutledge-Jonker, S., Swart, D., Kruit, R. W., Krol, M., van Pul, W., and de Arellano, J. V.-G.: Unraveling the diurnal atmospheric ammonia budget of a prototypical convective boundary layer, *Atmospheric Environment*, 249, 118 153, 2021.
- Seibt, U., Brand, W. A., Heimann, M., Lloyd, J., Severinghaus, J. P., and Wingate, L.: Observations of O<sub>2</sub> : CO<sub>2</sub> exchange ratios during ecosystem gas exchange, *Global Biogeochemical Cycles*, 18, 1–18, <https://doi.org/10.1029/2004GB002242>, 2004.
- 830 Severinghaus, J. P.: Studies of the Terrestrial O<sub>2</sub> and Carbon Cycles in Sand Dune Gases and in Biosphere, Ph.D. thesis, Columbia University, <https://doi.org/10.2172/477735>, 1995.
- Stephens, B. B., Keeling, R. F., Heimann, M., Six, K. D., Murnane, R., and Caldeira, K.: Testing global ocean carbon cycle models using measurements of atmospheric O<sub>2</sub> and CO<sub>2</sub> concentration, *Global Biogeochemical Cycles*, 12, 213–230, <https://doi.org/10.1029/97GB03500>, 1998.

- 835 Stephens, B. B., Bakwin, P. S., Tans, P. P., Teclaw, R. M., and Baumann, D. D.: Application of a differential fuel-cell analyzer for measuring atmospheric oxygen variations, *Journal of atmospheric and oceanic technology*, 24, 82–94, 2007.
- Stephens, B. B., Morgan, E. J., Bent, J. D., Keeling, R. F., Watt, A. S., Shertz, S. R., and Daube, B. C.: Airborne measurements of oxygen concentration from the surface to the lower stratosphere and pole to pole, *Atmospheric Measurement Techniques*, 14, 2543–2574, 2021.
- Sturm, P., Leuenberger, M., and Schmidt, M.: Atmospheric O<sub>2</sub>, CO<sub>2</sub> and  $\delta^{13}\text{C}$  observations from the remote sites Jungfrauoch, Switzerland, 840 and Puy de Dôme, France, *Geophysical research letters*, 32, 2005.
- Tennekes, H.: A model for the dynamics of the inversion above a convective boundary layer, *Journal of Atmospheric sciences*, 30, 558–567, 1973.
- Tohjima, Y., Mukai, H., Machida, T., Hoshina, Y., and Nakaoka, S.-I.: Global carbon budgets estimated from atmospheric  $\delta\text{O}_2/\text{N}_2$  and CO<sub>2</sub> observations in the western Pacific region over a 15-year period, *Atmospheric Chemistry and Physics*, 19, 9269–9285, 2019.
- 845 van der Laan, S., Van der Laan-Luijkx, I., Rödenbeck, C., Varlagin, A., Shironya, I., Neubert, R., Ramonet, M., and Meijer, H.: Atmospheric CO<sub>2</sub>,  $\delta$  (O<sub>2</sub>/N<sub>2</sub>), APO and oxidative ratios from aircraft flask samples over Fyodorovskoye, Western Russia, *Atmospheric environment*, 97, 174–181, 2014.
- van Heerwaarden, C. C. and Teuling, A. J.: Disentangling the response of forest and grassland energy exchange to heatwaves under idealized land–atmosphere coupling, *Biogeosciences*, 11, 6159–6171, 2014.
- 850 Vilà-Guerau de Arellano, J., Gioli, B., Miglietta, F., Jonker, H. J., Baltink, H. K., Hutjes, R. W., and Holtslag, A. A.: Entrainment process of carbon dioxide in the atmospheric boundary layer, *Journal of Geophysical Research: Atmospheres*, 109, 2004.
- Vilà-Guerau de Arellano, J., Van Heerwaarden, C. C., and Lelieveld, J.: Modelled suppression of boundary-layer clouds by plants in a CO<sub>2</sub>-rich atmosphere, *Nature geoscience*, 5, 701–704, 2012.
- Vilà-Guerau de Arellano, J., van Heerwaarden, C. C., van Stratum, B. J., and van den Dries, K.: Atmospheric boundary layer: Integrating air 855 chemistry and land interactions, Cambridge University Press, 2015.
- Vilà-Guerau de Arellano, J., Koren, G., Ouwersloot, H. G., van der Velde, I., Röckmann, T., and Miller, J. B.: Sub-diurnal variability of the carbon dioxide and water vapor isotopologues at the field observational scale, *Agricultural and Forest Meteorology*, 275, 114–135, 2019.
- Visser, A. J., Ganzeveld, L. N., Goded, I., Krol, M. C., Mammarella, I., Manca, G., and Boersma, K. F.: Ozone deposition impact assessments for forest canopies require accurate ozone flux partitioning on diurnal timescales, *Atmospheric Chemistry and Physics*, 21, 18 393–18 411, 860 2021.
- Wehr, R., Munger, J., McManus, J., Nelson, D., Zahniser, M., Davidson, E., Wofsy, S., and Saleska, S.: Seasonality of temperate forest photosynthesis and daytime respiration, *Nature*, 534, 680–683, 2016.
- Whelan, M. E., Lennartz, S. T., Gimeno, T. E., Wehr, R., Wohlfahrt, G., Wang, Y., Kooijmans, L. M., Hilton, T. W., Belviso, S., Peylin, P., et al.: Reviews and syntheses: Carbonyl sulfide as a multi-scale tracer for carbon and water cycles, *Biogeosciences*, 15, 3625–3657, 2018.
- 865 Worrall, F., Clay, G. D., Masiello, C. A., and Mynheer, G.: Estimating the oxidative ratio of the global terrestrial biosphere carbon, *Biogeochemistry*, 115, 23–32, 2013.
- Yan, Y., Klosterhalfen, A., Moyano, F., Cuntz, M., Manning, A. C., and Knohl, A.: A modeling approach to investigate drivers, variability and uncertainties in O<sub>2</sub> fluxes and O<sub>2</sub>: CO<sub>2</sub> exchange ratios in a temperate forest, *Biogeosciences*, 20, 4087–4107, 2023.